Electronic Supplementary Material (ESI) for Dalton Transactions.

(Ar–CO–C≡C)(PEt_3)Au and (Ar–C≡C)(PEt_3)Au complexes bearing pyrenyl and ferrocenyl groups: Synthesis, structures and luminescence properties

Marta Głodek,[a] *Anna Makal,*[b] *Piotr Paluch,*[c] *Mariola Kadziołka-Gaweł,*[d] *Yasuhiro Kobayashi,*[e] *Janusz Zakrzewski,*[a] *and Damian Plażuk*[a]*

[a] Department of Organic Chemistry, Faculty of Chemistry, University of Łódź, Tamka 12, 91-403 Łódź, Poland. Fax: (+48)42 6786583; Tel: (+48)42 6355760;

[b] University of Warsaw, Biological and Chemical Research Centre, ul. Żwirki i Wigury 101, 02-096 Warsaw, Poland

[c] Centre of Molecular and Macromolecular Studies, Polish Academy of Sciences, Sienkiewicza 112, 90-363 Łódź, Poland

[d] Institute of Physics, University of Silesia in Katowice, 75 Pułku Piechoty 1a, 41-500 Chorzów, Poland

[e] Research Reactor Institute, Kyoto University, Asashiro-nishi, Kumatori-cho, Osaka-fu 590-0494, Japan

Synthesis of ^{13}C-labeled compounds

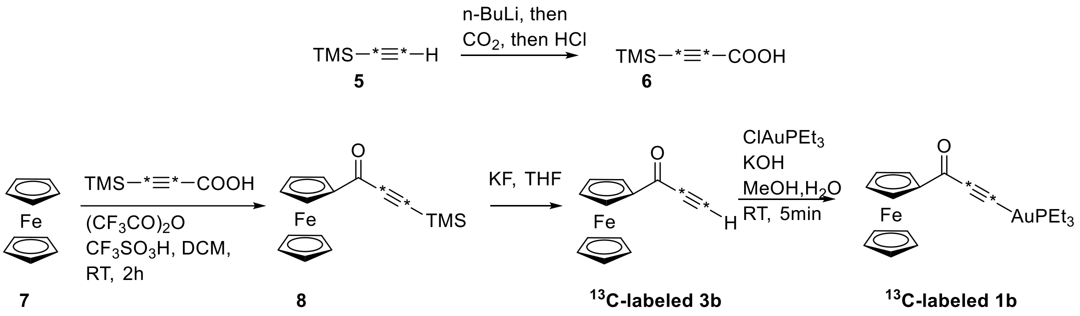

Scheme S1. Synthesis of ^{13}C-labeled gold(I) complex **1b**

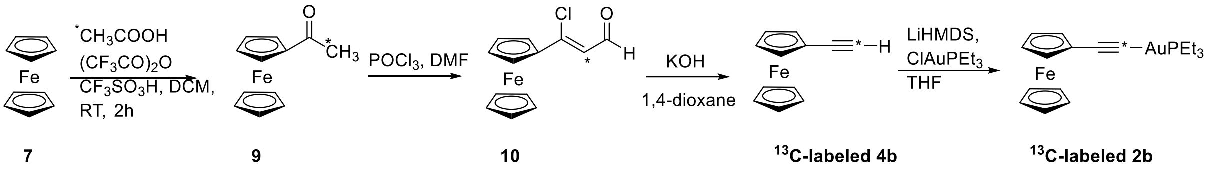

Scheme S2. Synthesis of ^{13}C-labeled gold(I) complex **2b**

3-(trimethylsilyl)propynoyl-2,3-^{13}C$_2$ acid 6. This compound was synthesized as described previously for TMSC≡CCOOH starting from TMS^{13}C≡^{13}CH instead of trimethylsiltlacetylene[1]. Crude product was used in a next step without further purification.

3-(trimethylsilyl)propynoyl-2,3-^{13}C$_2$-ferrocene 8. This compound was synthesized as described previously for non ^{13}C non-labeled **8**[2] starting from **6**. Crude product was used in a next step without further purification.

propynoyl-2,3-^{13}C$_2$-ferrocene ^{13}C-labeled-**3b .** This compound was synthesized as described previously for **3b** starting from **8**. Crude product was used in a next step without further purification.

^{13}C-labeled 1b. This compound was synthesized according to **1b** starting from ^{13}C-labeled **3b**. NMR spectra of a mixture of ^{13}C-labeled **1b** and ^{13}C-labeled **1b'**. ^{31}P{^{1}H} NMR (CD$_3$CN) δ 46.5 (s), 39.1 (dd, $^{2}J_{\text{P-C}}$=135.8, $^{3}J_{\text{P-C}}$=23.6 Hz, C(O)-^{13}C≡^{13}C-Au-P)

Acetylferrocene-2-^{13}C 9. This compound was synthesized in 95% yield (1.83 g) according to slightly modified known methodology of synthesis of acetylferrocene**.** starting from 1.57g (8.4 mmol) of ferrocene, 0.556 g (0.530 ml) of acetic-2-^{13}C acid, 1.26 ml of trifluoroacetic anhydride, and 0.80 ml of trifluoromethanesulfonic acid. Chromatography on silica using dichloromethane - hexane 7 - 3 as eluent gave pure **9** as red solid. ^{1}H NMR ($CDCl_3$) δ 4.77 (t, J=1.9 Hz, 2H, Cp), 4.50 (t, J=1.9 Hz, 2H, Cp), 4.02 (s, 5H, Cp), 2.39 (d, $^1J_{H\text{-}C}$=127.2 Hz, 3H, CH_3); $^{13}C\{^1H\}$ NMR ($CDCl_3$) δ 202.0 (d, $^1J_{C\text{-}C}$=42.8 Hz, C=O), 79.4 (d, $^2J_{C\text{-}C}$=15.4 Hz, Cp_{ipso}), 72.3 (Cp), 69.9 (Cp), 69.6 (Cp), 27.4 (*CH_3);

3-chloro-3-ferrocenylacrylaldehyde-3-^{13}C 10. This compound was synthesized in 26% yield (540 mg) according to known[3] methodology starting from 1.74 g (7.6 mmol) of **9**, 5 ml of phosphorus(V) oxychloride and 4.3 ml + 70 ml (as a solvent) of N,N-dimethylformamide. Chromatography on silica using gradient of dichloromethane - n-hexane starting from 1 - 1 to 3 - 1 led to pure **10** which solidified in a fridge. ^{1}H NMR ($CDCl_3$) δ 10.10 (dd, $^2J_{H\text{-}C}$=24.7, $^3J_{H\text{-}H}$=6.2 Hz, 1H, $C\underline{H}O$), 6.39 (dd, $^1J_{H\text{-}C}$=160.8 Hz, $^3J_{H\text{-}H}$=7.1 Hz, 1H, =$^{13}C\underline{H}$-CHO), 4.75 (br s, 2H, Cp), 4.56 (br s, 2H, Cp), 4.24 (s, 5H, Cp); $^{13}C\{^1H\}$ NMR ($CDCl_3$) δ 190.7 (d, $^1J_{C\text{-}C}$=59.4 Hz, $\underline{C}HO$), 155.1 (d, $^1J_{C\text{-}C}$=76.9 Hz, $\underline{C}$(Cl)=^{13}C-), 128.4 (=$C^{13}\underline{C}$-CHO), 120.4 ($C^{13}\underline{C}$-CHO), 80.1 (d, $^2J_{C\text{-}C}$=4.0 Hz, Cp_{ipso}), 72.2 (Cp), 70.9 (Cp), 68.8 (d, $^3J_{C\text{-}C}$=2.0 Hz, Cp)

(ethynyl-2-^{13}C)ferrocene ^{13}C-labeled-**4b.** This compound was synthesized in 17% yield (60 mg) according to known[3] methodology of synthesis of ethynylferrocene starting from 452 mg (1.64 mmol) of FcC(Cl)=^{13}CH-CHO **10** and 292 mg of KOH. Crude product was purified twice by chromatography on silica using n-hexane following by 1 - 1 dichloromethane - n-hexane as eluents. Pure ^{13}C-labeled **4b** was obtained as an orange oil. ^{1}H NMR ($CDCl_3$) δ 4.46 (t, J=1.8

Hz, Cp), 4.20 (t, *J*=1.8 Hz, 2H, Cp), 2.71 (d, $^{1}J_{\text{H-C}}$=250.3 Hz, $\text{C}\equiv{}^{13}\text{C}\underline{\text{H}}$); $^{13}\text{C}\{^{1}\text{H}\}$ NMR (CDCl_3) δ 108.5 ($\underline{\text{C}}\equiv{}^{13}\text{CH}$), 73.5 ($\underline{\text{C}}\equiv{}^{13}\underline{\text{C}}\text{H}$), 71.8 (d, $^{3}J_{\text{C-C}}$=2.1 Hz, Cp), 70.0 (Cp), 68.7 (Cp)

^{13}C-labeled-**2b.** This compound was synthesized in 20% yield (30 mg) according to **2b** starting from 60 mg of ^{13}C-labeled **4b** (0.284 mmol), 99.6 mg of ClAuPEt_3 (0.284 mmol), and 0.284 ml of LiHMDS (c=1M). Crystallization from a mixture of ethyl acetate – n-heptane gave pure product as dark orange crystals. ^{1}H NMR (CD_3CN) δ 4.26 (t, *J*=1.8 Hz, 2H, Cp), 4.13 (s, 5H, Cp), 4.10 (t, *J*=1.8 Hz, 2H, Cp), 1.86 (qd, *J*=9.9, 7.7 Hz, 6H, $\text{C}\underline{\text{H}}_2\text{CH}_3$), 1.17 (dt, *J*=18.1, 7.7 Hz, 9H, $\text{CH}_2\text{C}\underline{\text{H}}_3$); $^{13}\text{C}\{^{1}\text{H}\}$ NMR (CD_3CN) δ 136.7 (d, $^{2}J_{\text{C-P}}$=140.1 Hz, $\text{C}\equiv{}^{13}\underline{\text{C}}$-Au-P), 75.2 ($\text{Cp}_{\text{ipso}}$), 72.1 (2xC, Cp), 70.7 (Cp), 68.7 (Cp), 18.5 (d, $^{1}J_{\text{C-P}}$=33.7 Hz, $\underline{\text{C}}\text{H}_2\text{CH}_3$), 9.6 ($\text{CH}_2\underline{\text{C}}\text{H}_3$); $^{31}\text{P}\{^{1}\text{H}\}$ NMR (CD_3CN) δ 39.6 (d, $^{2}J_{\text{P-C}}$=140.4 Hz)

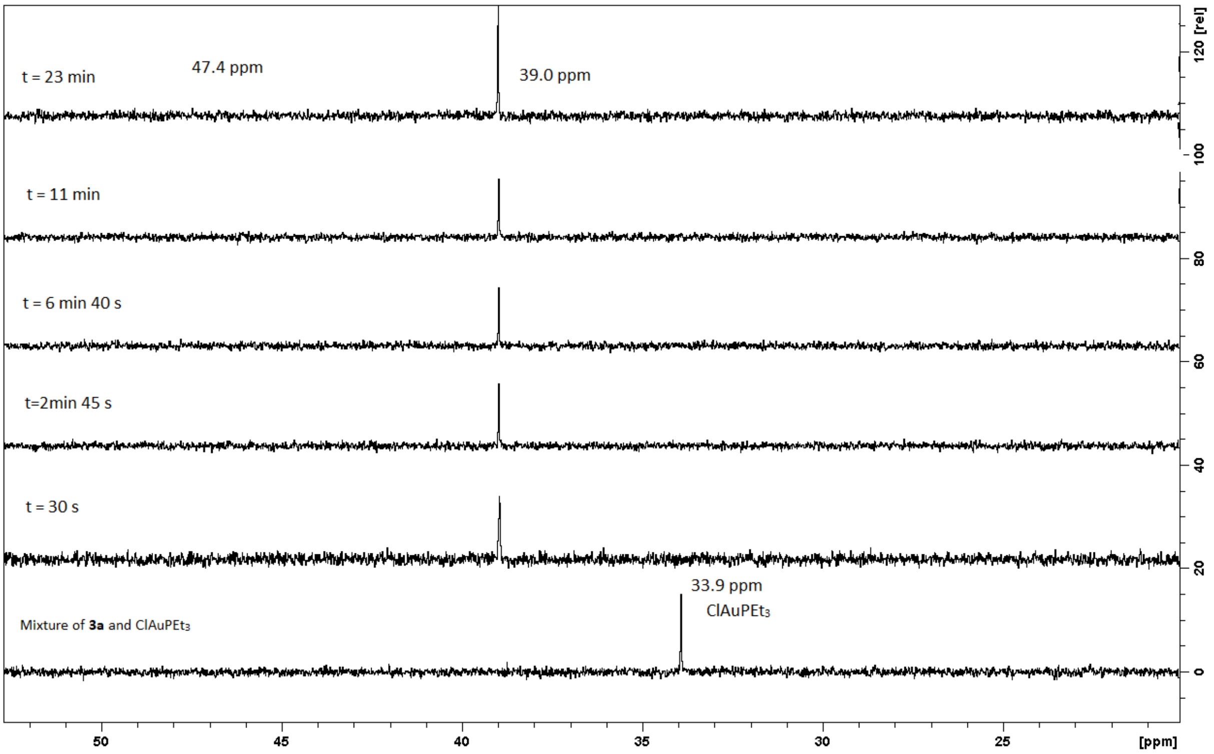

Fig. S1. ${}^{31}P\{{}^{1}H\}$ -monitored reaction of **3a** with $ClAuPEt_3$ in CD_3OD at 303 K.

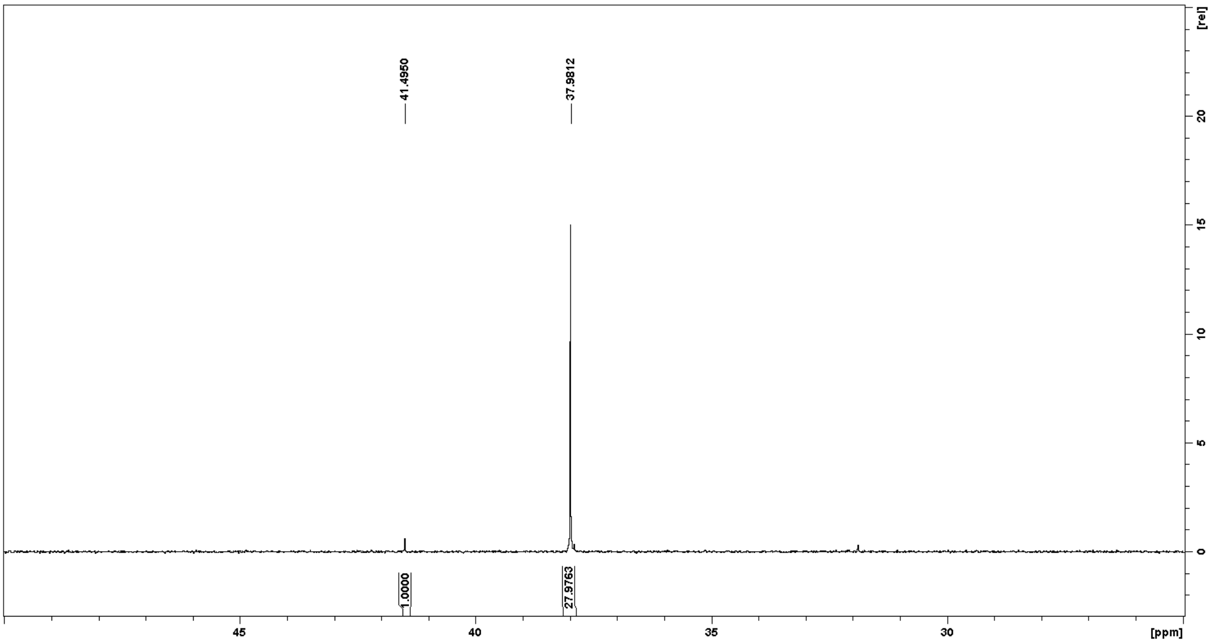

Fig. S2. ${}^{31}P\{{}^{1}H\}$ NMR spectra of freshly prepared CD_2Cl_2 solution of **1a** (1st fraction)

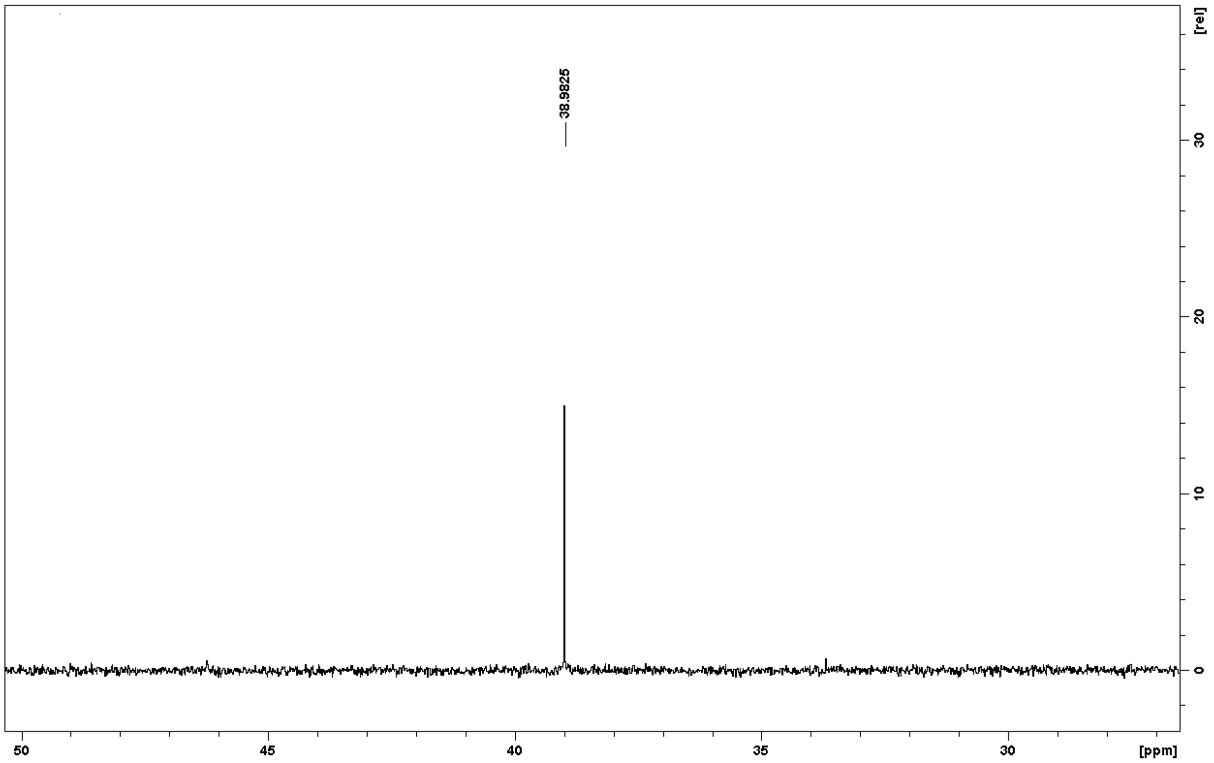

Fig. S3. $^{31}P\{^1H\}$ NMR spectra of freshly prepared CD_3CN solution of **1a** (1st fraction)

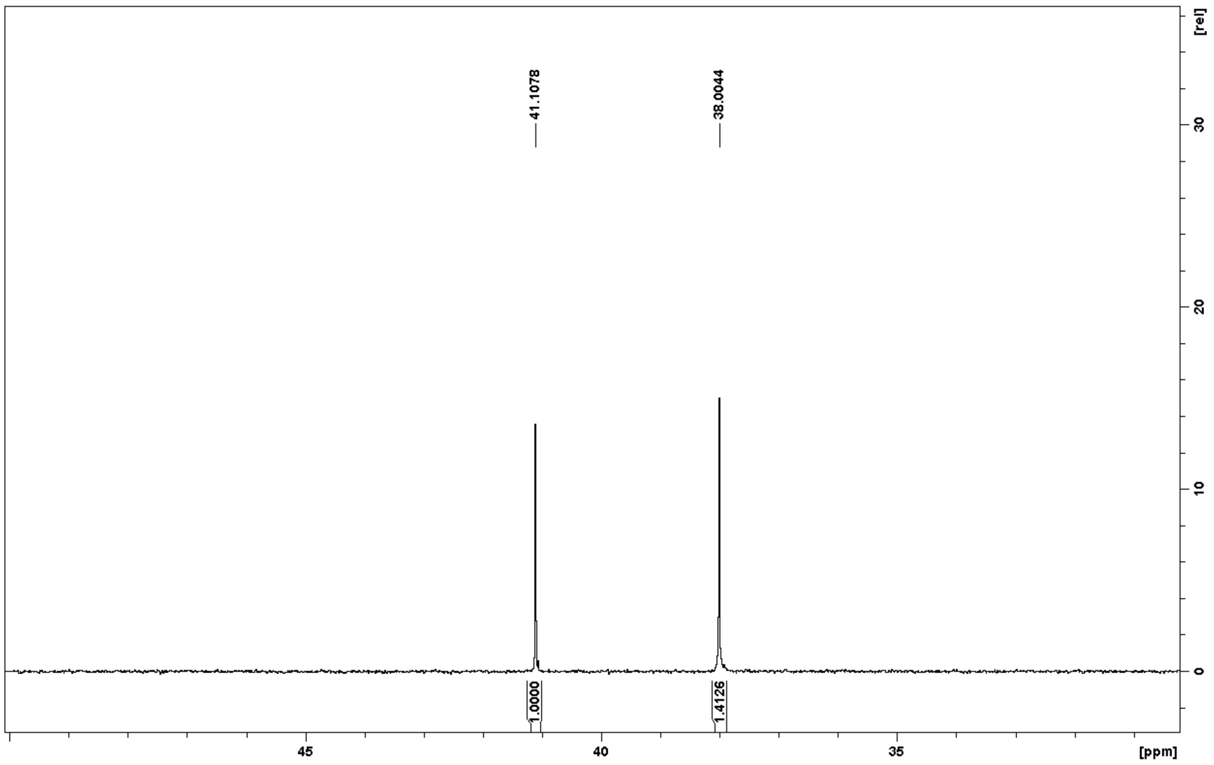

Fig. S4. $^{31}P\{^1H\}$ NMR spectra of freshly prepared CD_2Cl_2 solution of **1a** (2nd fraction)

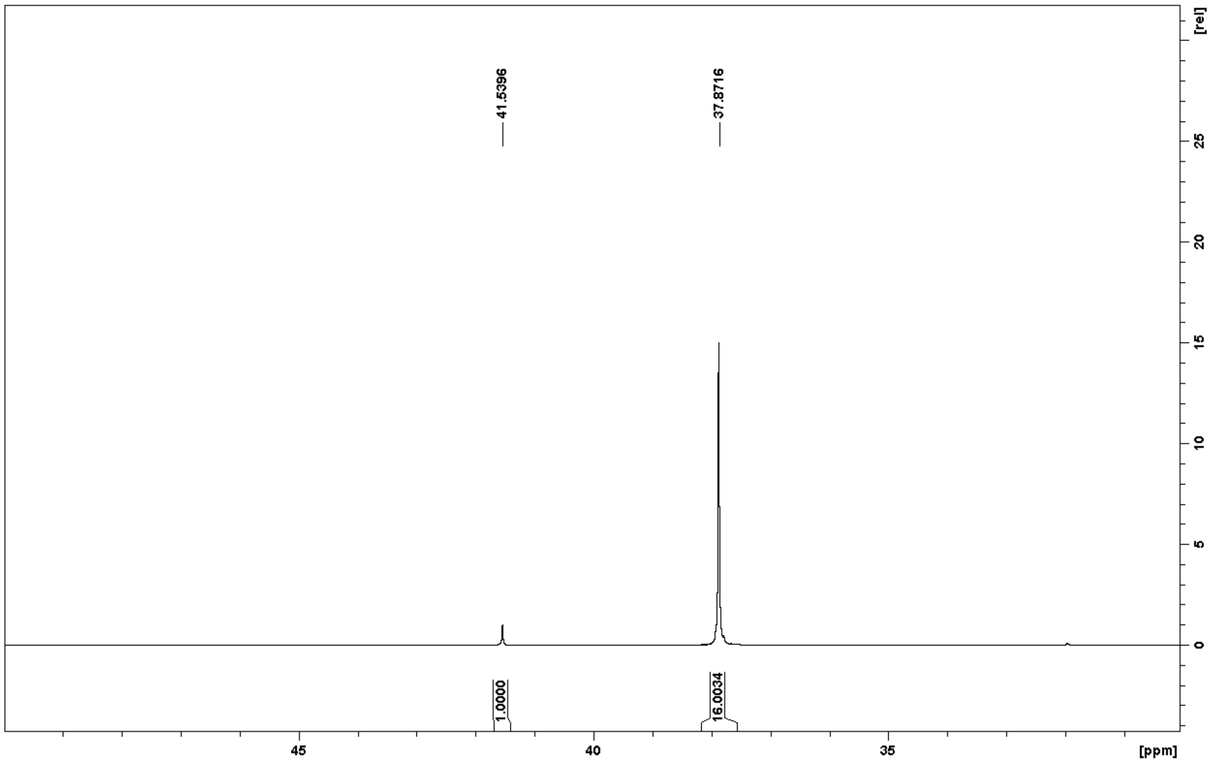

Fig. S5. $^{31}P\{^1H\}$ NMR spectra of freshly prepared CD_2Cl_2 solution of **1b** (1st fraction)

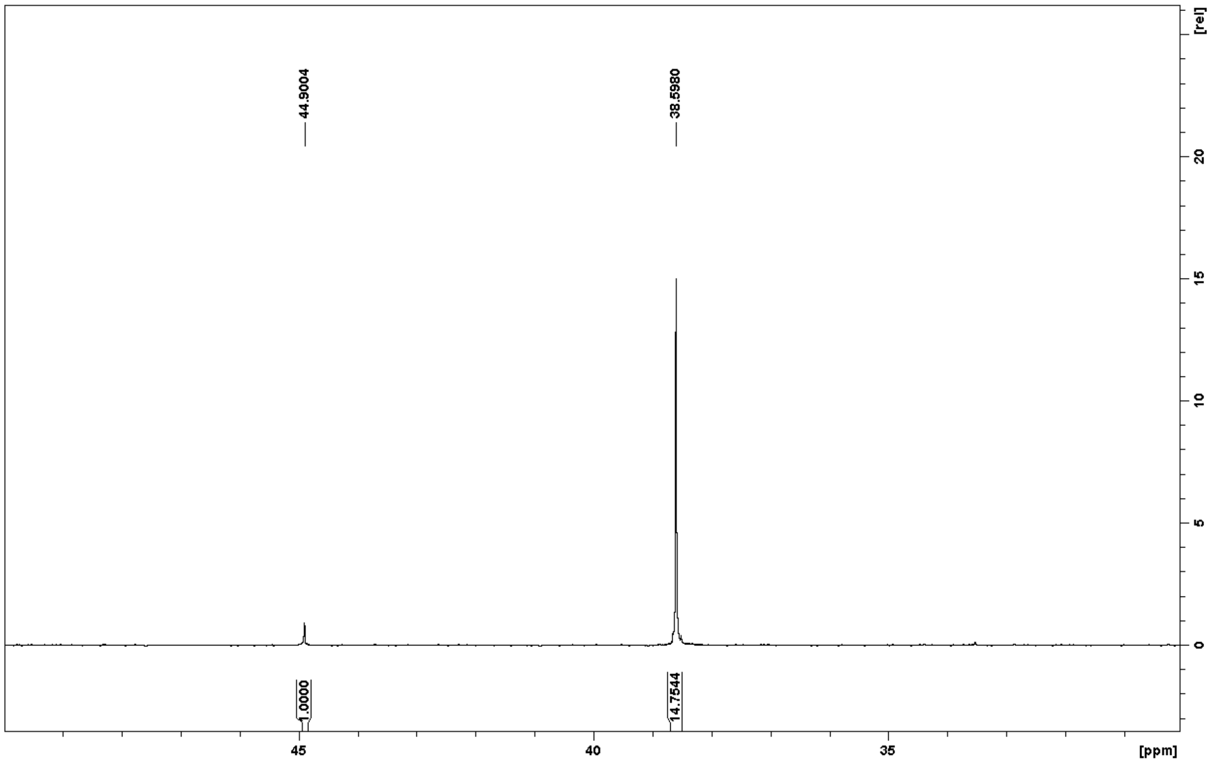

Fig. S6. $^{31}P\{^1H\}$ NMR spectra of freshly prepared CD_3CN solution of **1b** (1st fraction)

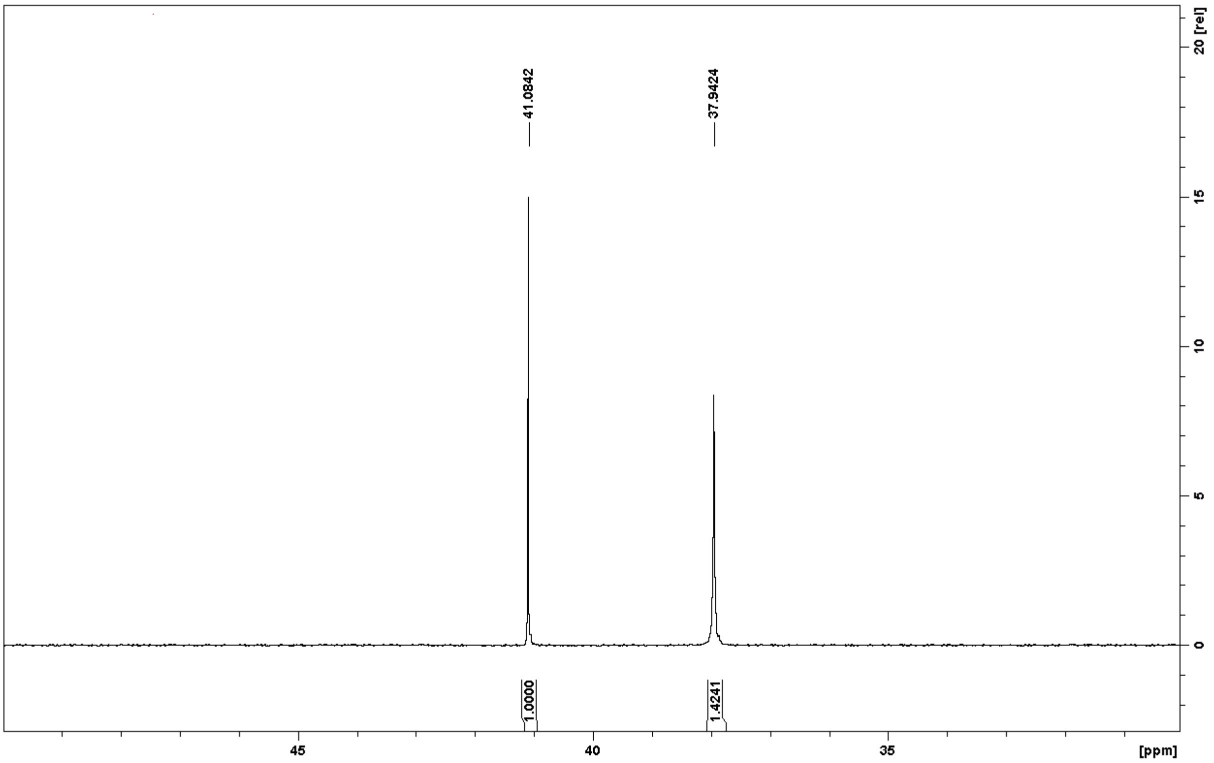

Fig. S7. $^{31}P\{^{1}H\}$ NMR spectra of freshly prepared CD_2Cl_2 solution of **1b** (2^{nd} fraction)

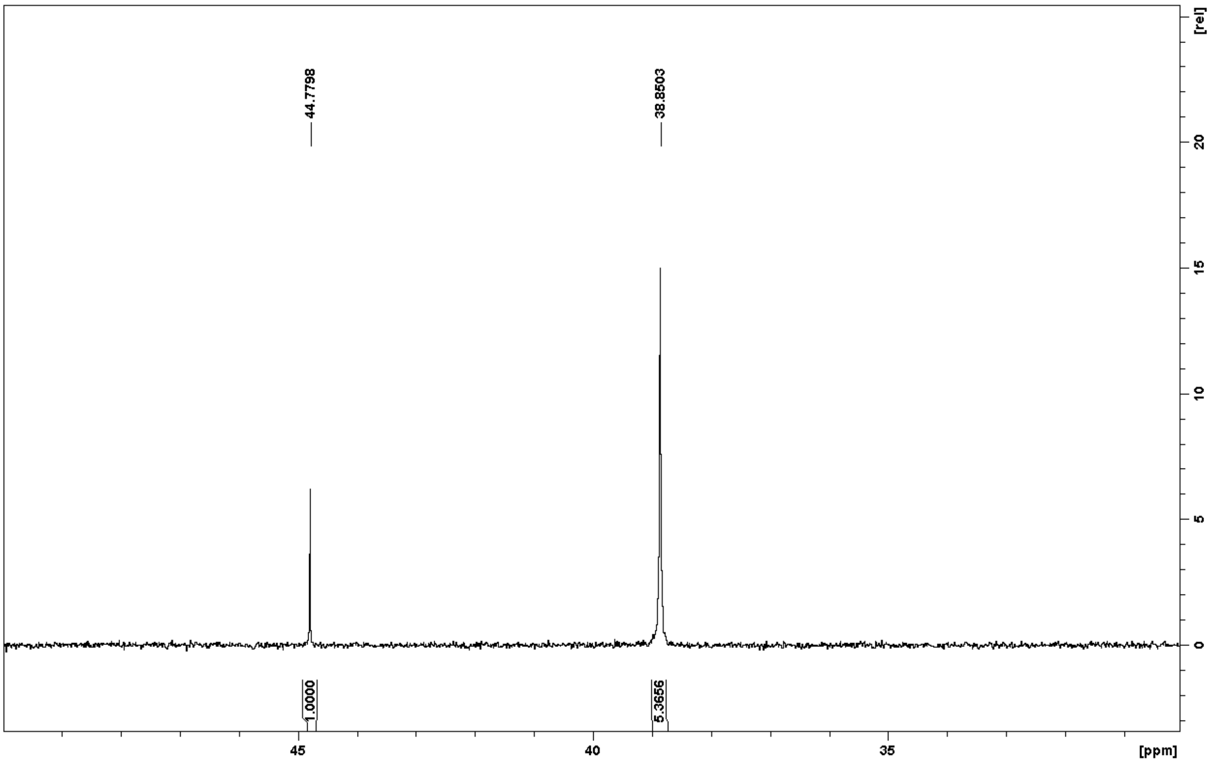

Fig. S8. $^{31}P\{^{1}H\}$ NMR spectra of freshly prepared CD_3CN solution of **1b** (2^{nd} fraction)

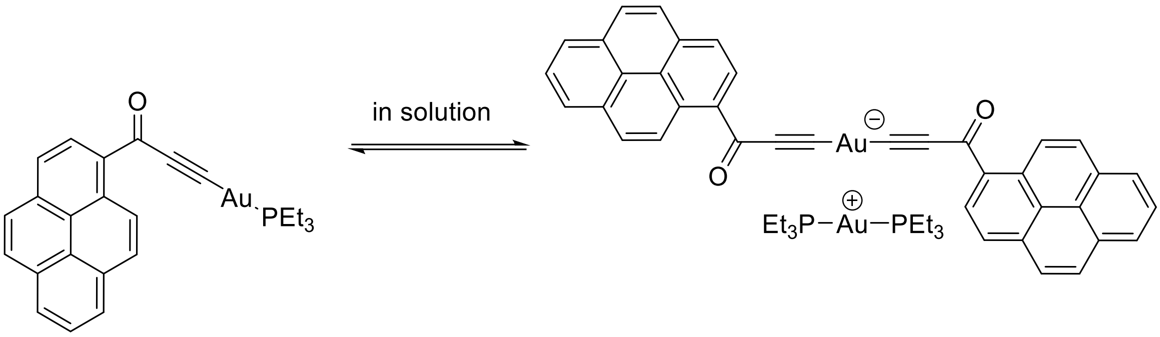

1a **1a'**

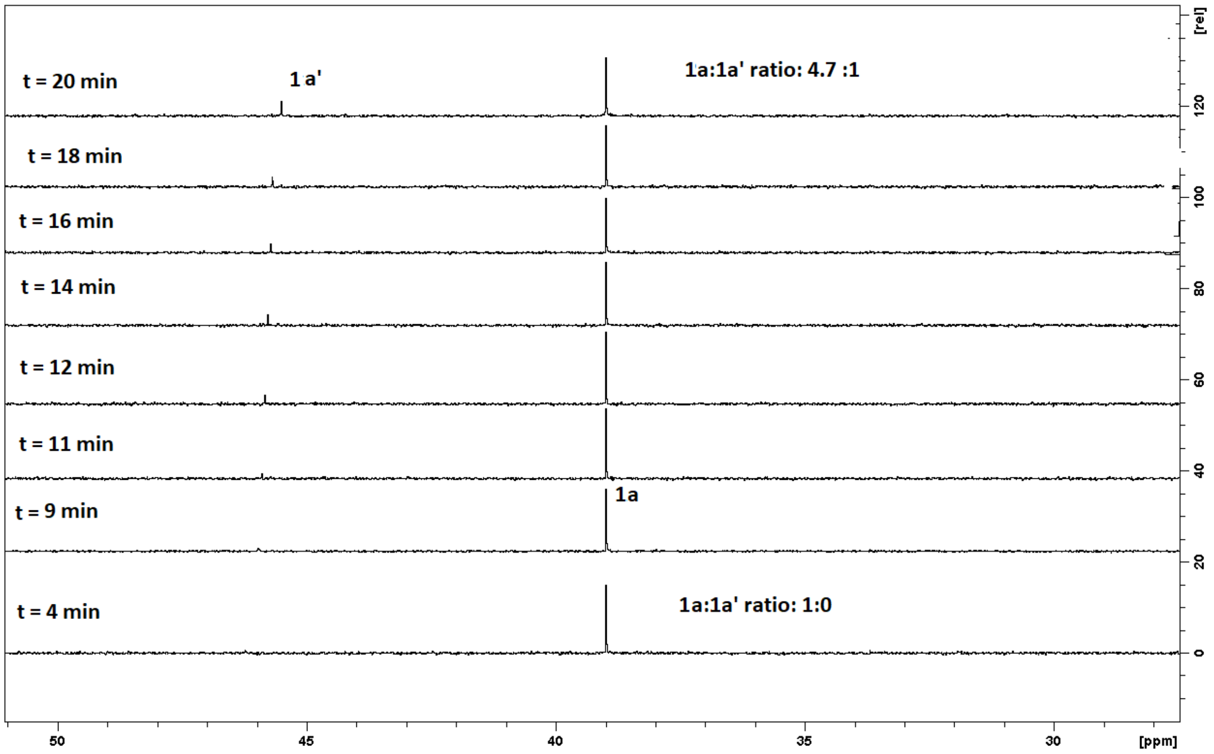

Fig. S9. Ligand scrambling in **1a** in CD_3CN solution. $^{31}P\{^{1}H\}$ spectra of saturated solution of **1a** in CD_3CN; peaks assignment: **1a** $\delta = 39.0$ ppm; **1a'** $\delta = 45.7$ ppm

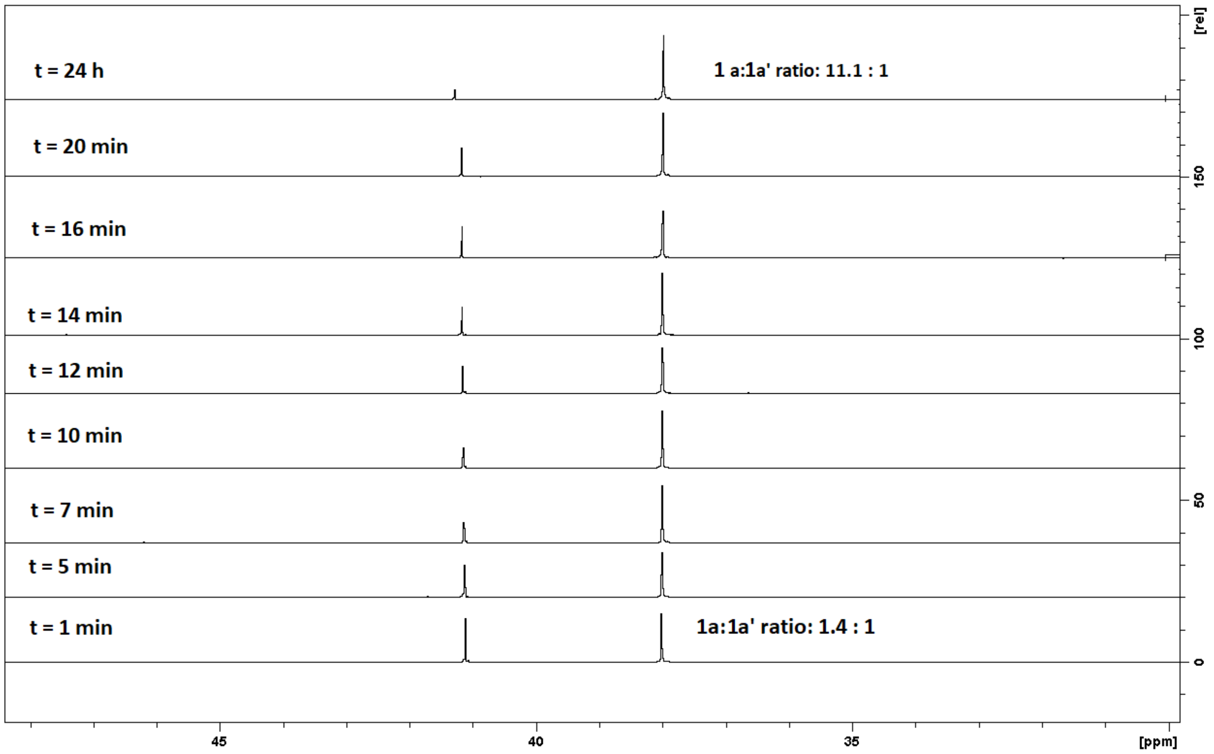

Fig. S10. Ligand scrambling in **1a'** in CD_2Cl_2 solution. $^{31}P\{^1H\}$ spectra of saturated solution of **1a'** in CD_2Cl_2; peaks assignment: **1a** δ = 39.0 ppm; **1a'** δ = 45.7 ppm

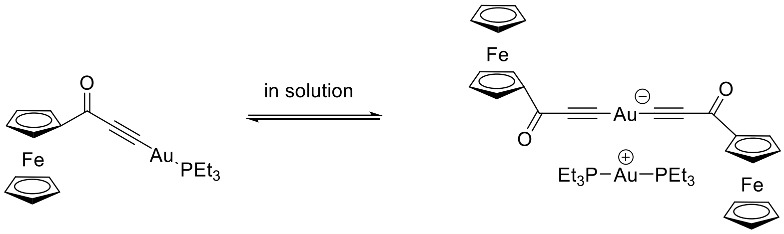

1b **1b'**

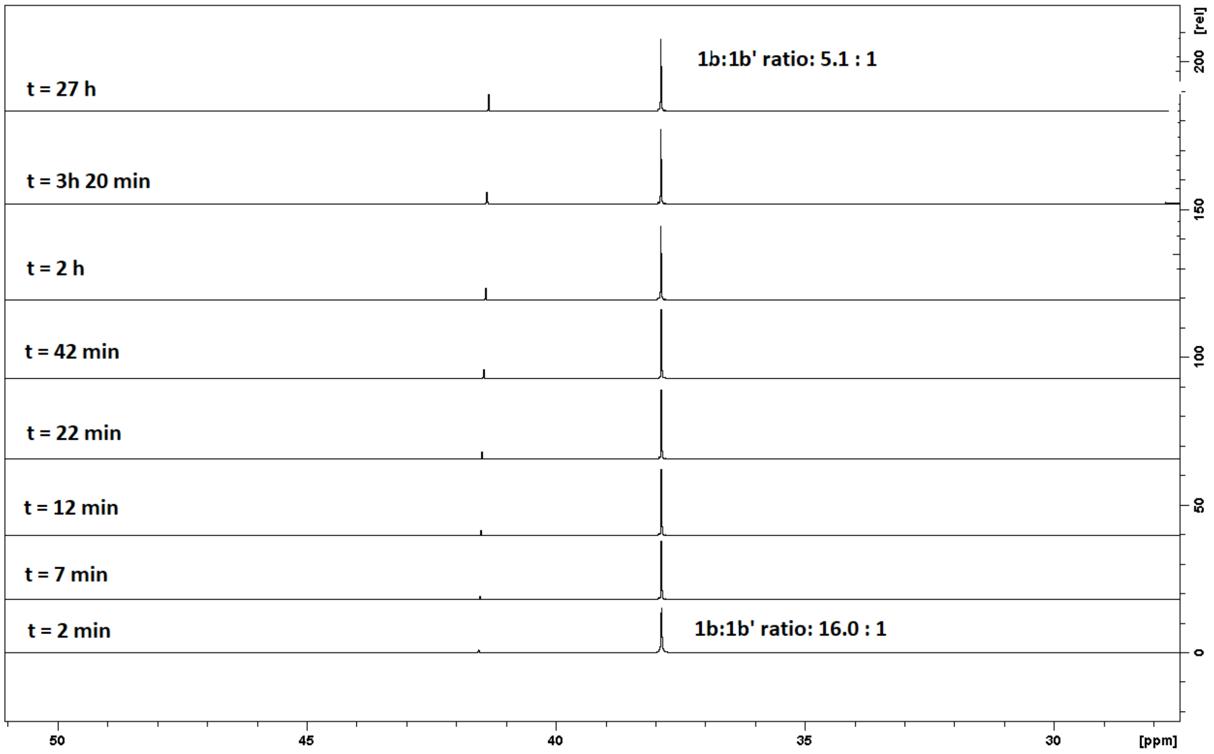

Fig. S11. Ligand scrambling in **1b** in CD_2Cl_2 solution. $^{31}P\{^1H\}$ spectra of saturated solution of **1b** in CD_2Cl_2; peaks assignment: **1b** δ = 37.9 ppm; **1b'** δ = 41.4 ppm

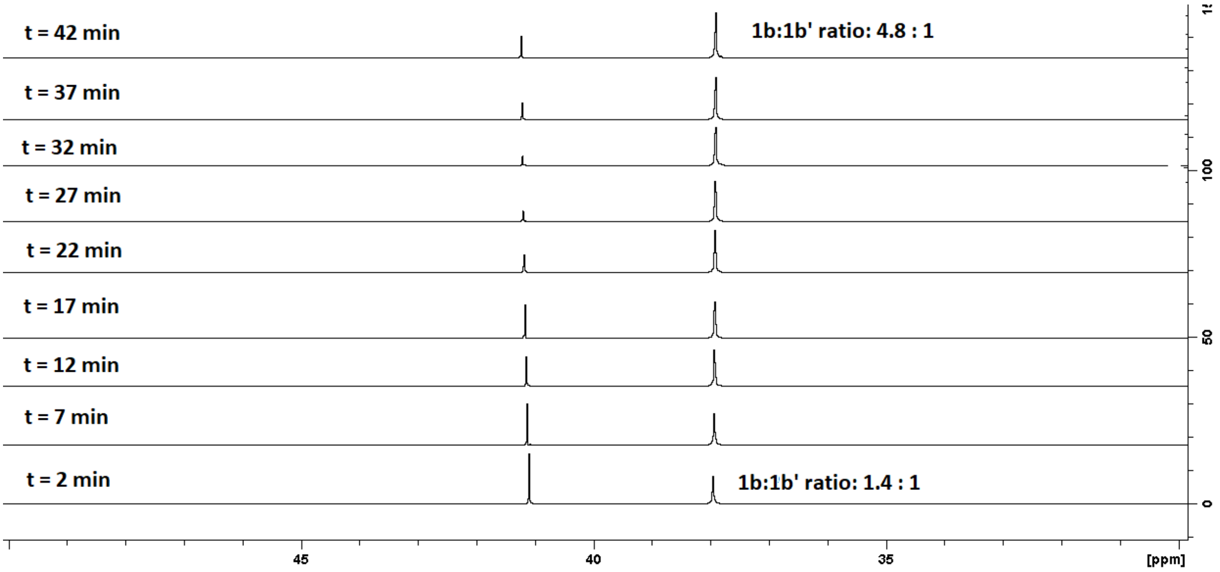

Fig. S12. Ligand scrambling in **1b'** in CD_2Cl_2 solution. $^{31}P\{^1H\}$ spectra of saturated solution of **1b'** in CD_2Cl_2; peaks assignment: **1b** δ = 37.9 ppm; **1b'** δ = 41.4 ppm

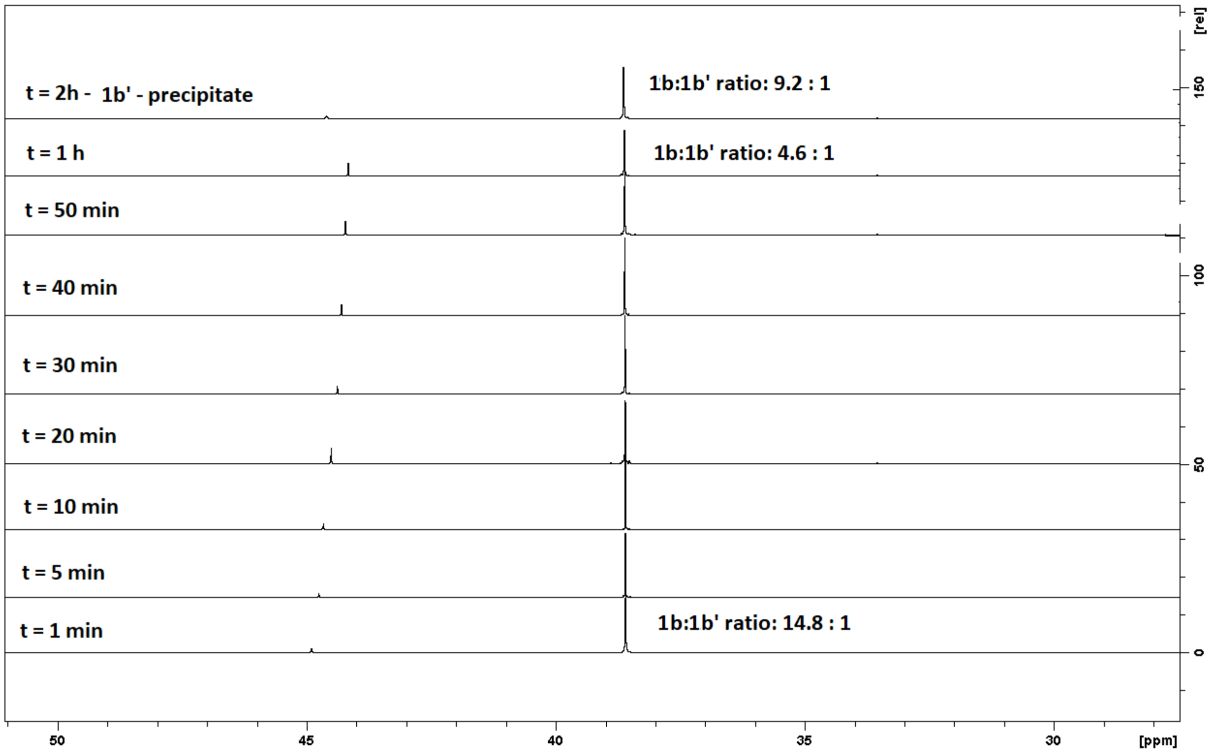

Fig. S13. Ligand scrambling in **1b** in CD_3CN solution. $^{31}P\{^1H\}$ spectra of saturated solution of **1b** in CD_3CN; peaks assignment: **1b** δ = 38.6 ppm; **1b'** δ = 44.9 ppm

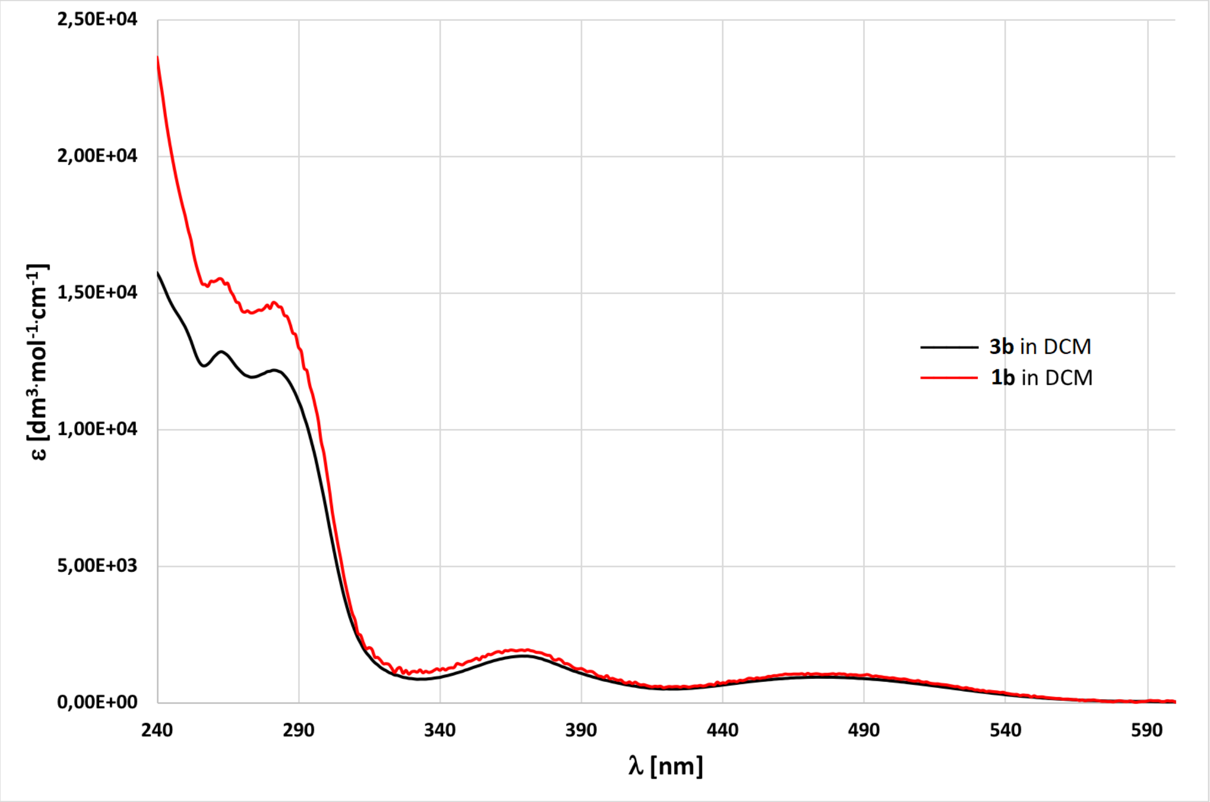

Fig. S14. UV-VIS absorption spectra of **1b** and **3b** in dichloromethane (DCM).

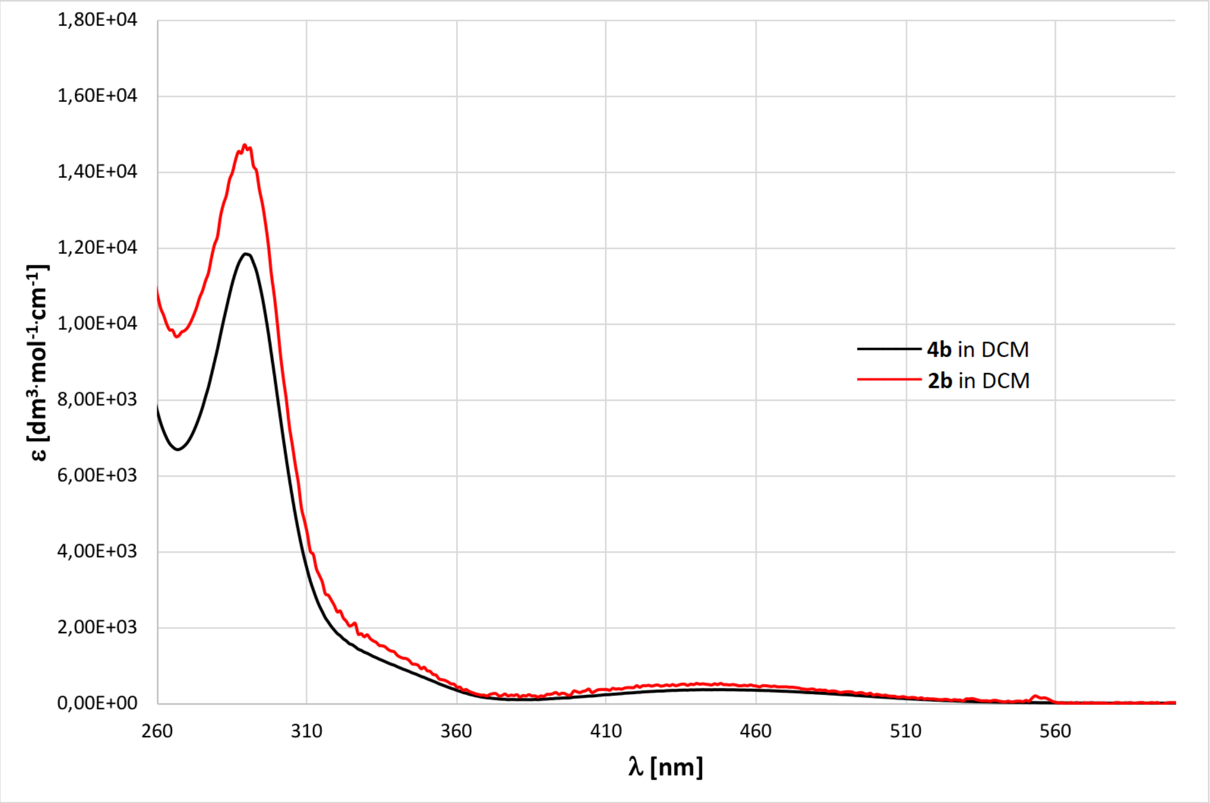

Fig. S15. UV-VIS absorption spectra of **2b** and **4b** in dichloromethane (DCM).

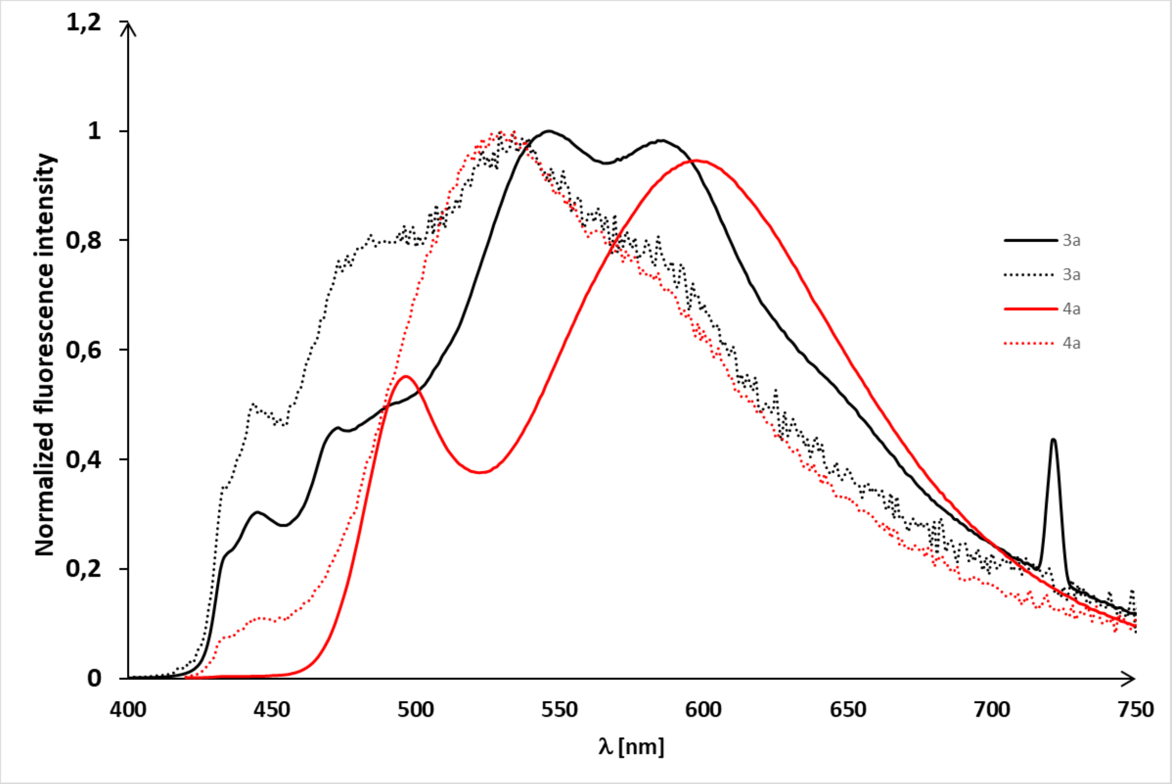

Fig. S16 Normalized solid state fluorescence spectra (solid lines) and delayed fluorescence spectra (delay time 50 μs) (dotted lines) for **3a** and **4a**

Table S1 UV-VIS absorption properties of **3b**, **4b** and gold(I) complexes **1b**, **2b**

Compound	λ_{max} [nm]; (ε [$dm^3 \cdot mol^{-1} \cdot cm^{-1}$])
1b	264 (15,050); 283 (14,600); 370 (2,050); 477 (1,100)
2b	250 (12,400); 290 (14,200); 445 (430)
3b	284 (7,800); 375 (1,550); 489 (1,160)
4b	267 (5,700); 333 (230); 445 (1,900)

X-ray diffraction analysis

The X-ray data for **1b'**, **2a** and **2b** were collected on BRUKER KAPPA APEX-II Ultra diffractometer, with molybdenum rotating anode as X-ray source and multi-layer focusing mirrors. The data were collected with Bruker APEX-II software[4], integrated using Bruker SAINT software package[5], and were corrected for absorption effects using the multi-scan method or numerical approach (SADABS[6]).

The data for compound **1a** and **1a'** were collected on Agilent Supernova 4 circle diffractometer system equipped with molybdenum microsource and Eos CCD detector. The data were collected with CrysAlis171[7] software and integrated with the same software. Data were corrected for absorption effects using the analytical absorption correction based on crystal faces (SCALE3 ABSPACK[7])

Low temperature of all the samples was maintained by keeping them in the cold nitrogen stream, using Oxford Cryosystems liquid nitrogen cooling device.

The structures of **1a**, **1b'**, **2a** and **2b** were solved by direct methods using SXELXS, while the structure of **1a'** was solved by charge flipping algorithm as implemented in Superflip program[8].

All structures were refined by full-matrix least squares procedure with SHELXL[9] within OLEX2[10] graphical interface. In all instances H atoms were visible in the residual density map, but were added geometrically and refined mostly in riding approximation. In the case of **1a'**, z coordinate of Au atoms was fixed at the final refinement stage, otherwise it showed small oscillations in the direction of the main Au···Au chain, preventing strict refinement convergence.

Figures were prepared with Ortep3v2[11] and Mercury_3.6[12] software.

Detailed information about the data processing, structure solution and refinement is presented in Table S2.

In the case of complexes **1a'** and **1b'**, there are multiple pyrenyl and ferrocenyl moieties were present in the crystallographic asymmetric unit. These will be further denoted as moieties I–IV (**1a'**) or I–II (**1b'**), depending on the number of the associated carbonyl O or Fe atoms. With respect to the geometry of the Au coordination, all of the considered compounds showed considerable similarity. The Au–P bond lengths were very similar irrespectively of the ligand following the ethynylarene/propynoyloarene moiety. A tendency for the Au–P bond to be slightly longer (i.e. more than 2.3Å) was observed in the cases of **1a'** and **1b'**, where longer chains of Au … Au … Au interactions were present, which might be the result of the steric strain on phosphine moieties.

The Au–$C_{(C\equiv C)}$ bond was uniformly very close to 2.0 Å, very similar to Au–$C_{(C\equiv N)}$[13] and $(PhC\equiv C)_2Au^-$ (18C6)K^+ (Au–$C_{(C\equiv N)}$ in a the range of 1.99 to 1.994Å)[14]. Unsurprisingly, the C≡C bond length was very uniform (Table S3) with a typical value of 1.21Å. The carbonyl moiety, where present, also showed the typical length for a double C=O bond. The $C_{C=O}$–$C_{C\equiv C}$ bond was uniformly ~ 1.45Å, suggesting a single bond. In the case of the bond connecting a pyrene or ferrocene ligand with the ethynyl/propynoyl fragments, its length was shorter than that of a typical single bond for compounds without a carbonyl moiety and the longest in the case of **1a'** and **1a**. The carbonyl moiety, where present, was rotated slightly above the plane of the Cp or pyrenyl ligand. This rotation was more pronounced in the case of pyrene derivatives **1a'** and **1a**, being on average ~17°, while in the case of **1b'**, the corresponding dihedral angle did not exceed 12° (Table S4). Compounds **1a**, **2a** and **2b** all showed a slight bent in the apparently linear coordination of Au(I), although the appropriate valence angles deviated from 180° by no more than 6° (Table S4). A ferrocene moiety was close to eclipsed conformation in both **1b'** and **2b**, with the relative rotation of two Cp rings of ~3° for **1b'** and ~ 10° for **2b** (Table

S6). The Cp–Fe distances were almost equal in all the instances, and the planes of the cyclopentadienyl rings were almost parallel (the angle between the planes was always ~ 3°).

The compound **2a** crystallized in monoclinic C 2/c. The Au coordination was linear, with bond lengths typical for the Au–C and Au–P bonds (Table S3). There was a very slight bent away from the pyrene plane, with the Au1 atom farthest out of plane and P1 almost exactly back in plane, as illustrated by Au … pyr_plane and P … pyr_plane distances in Table S3. All of the three ethyl moieties of the phosphine were roughly coplanar and oriented clockwise. The C19-containing ethyl group was almost parallel to the pyrene plane (Table S4). Compound **2a** formed a dimer of the L–Au–PEt_3 moieties, related to the crystallographic $2_{[010]}$ axis, and bound by the Au … Au interaction. The dimer was formed so that the pyrene planes were almost exactly perpendicular, as illustrated by P1–Au1–Au1–P1 dihedral angle (89.87(2)°), and both L–Au–PEt_3 linear fragments were almost perpendicular to the Au … Au bond, the Au1–Au1–C18 angle being 83.36(5)° and the Au1–Au1–P1 angle being ~ 100° (Table 4). The Au … Au distance was relatively short (Table S5), indicating a tendency to aurophilic interactions.

The most important interaction that seemed to determine the crystal packing was the pairwise π-stacking of pyrene systems related by crystallographic translation, although the inter planar distance between the stacked moieties was rather long, 3.512(6) Å. The shortest resulting interatomic contact is that of C6 … C12 3.476(6)Å. The dimers connected by π-stacking formed a wavy ribbon (Fig. S20). Consecutive chains were stacked one above the other along the crystallographic [010] direction, forming a layer, stabilized by C–H … π interactions of ethyl groups with the exposed pyrene plane. Such layers were then stacked along crystallographic [001] direction so that the Au–PEt_3 fragments formed bands in the bc plane, interspersed by bands of pyrene moieties (Fig. S21). In contrast to **2a**, the ferrocenyl complex **2b** crystallized without any trace of aurophilic interactions in the crystal lattice (Fig. S24). It remained 'monomeric' and crystallized in the highly symmetric Pbca space group. The L–C≡C–Au–P line was slightly bent above the cyclopentadienyl plane, with the P1 atom being the furthest above the plane. One of the Et-s was almost parallel to Cp1 of the three ethyl moieties in phosphine, and the second was bent counterclockwise and almost coplanar, while the third is pointed along the Au1–P2 bond. The major packing motif was a ribbon of **2b** monomers, related by the crystallographic $b_{[100]}$ plane, stacked in the [010] direction such that the adjacent ferrocene moieties were oriented almost perpendicularly to each other, and a short intermolecular Au1 … H2 contact of 2.853(6) Å was formed (Fig. S20). These ribbons were then stacked on top of one another in the crystallographic [100] and [001] directions, forming bands of Au–PEt_3 fragments interspersed with bands of ferrocene moieties.

In contrast to (acetylide)gold(I) complexes **2a** and **2b**, (aryoylacetylide)gold(I) complexes **1a** and **1b** formed, *via* ligand scrambling, two forms, both in solution and in the solid state. Compound **1a** crystallized in the monoclinic system, essentially in the monomeric form. The Au atom formed the closest contacts with the hydrogen atoms from the surrounding ethyl moieties. The pyrene moiety in **1a** was flat and was not coplanar with the propynoyl moiety which was rotated away from the pyrene plane. The L–(C=O)–C≡C–Au–P fragment showed the least discrepancies from linearity among the described structures. All the three ethyl fragments of the PEt_3 were roughly coplanar with one another and pointed counterclockwise. There were pyrene … pyrene π-stacked dimers formed by molecules related by the crystallographic center of inversion, but the average distance between the two pyrene planes was rather large, 3.581(5)Å (Fig. S23) which was in contrast to **1a'**, where the distances between the π-stacked pyrene planes were on average shorter than 3.4Å.

The dimers of **1a** were lined parallel to [010], therefore, the pyrene edges of one dimer could point in between the pyrene moieties in the adjacent dimer, and some C–H … O contacts could be formed. Similarly, the other sandwiched **1a** dimers were placed along [001] and oriented such that the pyrene edges pointed in between the sandwiched pyrene fragments from the previous layer, which maximized the C–H … π contacts of the ethyl moieties with exposed pyrene planes. In the [100] direction, packing seemed to be governed by C–H … π and possibly the C–H … Au interactions. Viewed along [010] or [001], the crystal structure consisted of pyrene layers interspersed by the Et–Au layers (Fig. S27).

While compound **1a** crystallized in the monoclinic system, **1a'** crystallized in the triclinic system. The compound formed a roughly infinite Au … Au … Au … chain along the [010] crystallographic direction, in which the Au atoms were coordinated either by two propynoylopyrene moieties or by two phosphine ligands.

A set of four Au atoms with their coordinating ligands constituted a crystallographic asymmetric unit and was thus referred to as a molecular stick. Two sets of L_2Au … $Au(PEt_3)_2$ fragments within the stick differed mainly in the conformations of the PEt_3 groups. In the first set, in both PEt_3 (P1 and P2 atoms), two ethyl groups were coplanar and rotated in the opposite direction, while a the third was almost collinear with the closest Au … Au bond and the atoms P1–Au2–P2 formed an almost ideal straight line (Table S5). In the second set, in both the phosphine moieties, all the ethyl groups were coplanar, two of them pointing counterclockwise and one clockwise, and the atoms P3 and P4 pointed away from the Au3–Au4 bond (Fig. 17 and Fig. 13(a)). The carbonyl groups were rotated slightly above the pyrene plane in the case of all the four independent groups. In the situations where two propynoylopyrene moieties were connected with the same Au atom, the carbonyl groups point in the opposite directions.

The coordination of Au(I) by either two propynoylopyrene substituents or two phosphines was linear (Table S5), however, the C≡C–Au–C≡C line was not perpendicular to the P–Au–P line, the dihedral angles between those lines varying from ~82° to ~71° (exact values provided in Table S5). Neither C≡C–Au–C≡C nor P–Au–P line was fully perpendicular to the direction of Au … Au … Au … chain, although the deviations of the Au–Au–C and Au–Au–P angles from 90° did not exceed 5°.

The crystal packing resulted in the first place from the close π-stacking of pyrene moieties from the adjacent sets of the Au … Au … Au … molecular sticks in the crystallographic c direction (Fig. S18). The anti-parallel pyrene moieties formed infinite stacks in the crystallographic [010] direction, parallel to the Au … Au … Au … Au sticks. In contrast to the Au atoms, which formed sets of four closely bound atoms, the distances between the pyrene planes within the stacks were very similar (Table S5), with the average value of 3.39Å. The molecular sticks, connected by π-stacking, form a flat layer stretching along the crystallographic [−101] direction (Fig. S23). The layers organized in a way that preserved bands of the Au(PEt$_3$)$_2$ groups interspersed with the bands of the pyrene moieties.

Similarly to **1a'**, its ferrocenyl analogue **1b'** crystallizes in a low symmetry triclinic system, and formed an infinite Au … Au … Au … chain along the crystallographic direction. The asymmetric unit was constituted by a heterodimer L$_2$Au … Au(PEt$_3$)$_2$. The carbonyl groups were rotated slightly above the Cp planes, while the C≡C–Au fragment points below the Cp1 plane. The two Cp rings connected by the $C_{C=O}$–C≡C–Au–C≡C–$C_{C=O}$ bridge were almost exactly parallel. However, one of the ferrocene moieties were rotated toward the Au(PEt$_3$)$_2$ group, another away from it, lowering the apparent chemical symmetry of the system and giving the complex a balance-like shape. The conformations of both the triethylphosphine ligands were similar to each other and to the P1 and P2 phosphine conformations in the **1a'** compound (two ethyl groups were coplanar and bent in the opposite directions; the third ethyl group was almost parallel to direction of the Au … Au interaction). The Au … Au distance within an asymmetric unit was relatively short, 3.2347(3)Å, approaching that characteristic for aurophilic interactions. This distance was slightly longer than the distances within the molecular stick of **1a'**; the 'interdimer' distances in the crystallographic a direction were, however, hardly longer (3.5813(3) Å). With all of the Au … Au vectors exactly parallel to the crystallographic [100] direction, as illustrated by the set of Au–Au–Au angles in Table S5 and Fig. 13, the compound formed truly infinite chains of Au …. Au …. Au … interactions, a 'molecular wire'. The coordination of Au(I) by either two 1-propynoylopyrene substituents or two phosphines was linear (Table S5), however, the C≡C–Au–C≡C line was not perpendicular to the P–Au–P line, the dihedral angle being ~76°, similar to **1a'** (exact value are given in Table S5). Neither the C≡C–Au–C≡C nor the P–Au–P line were fully perpendicular to the direction of the Au … Au … Au … chain. While the phosphine substituents were almost perpendicular to the Au … Au direction, the C≡C–Au–C≡C line was significantly tilted, with the Au2–Au1–C13 and the Au2–Au1 - C33 angles being ~103° and ~76°, respectively. This is to accommodate the conformations of both ferrocene moieties. Similarly to **1a'**, the Au atoms, apart from the closest coordinating ligands, are surrounded by H atoms from the ethyl groups.

Overall crystal packing of **1b'** was very similar to that of **1a'**. A parallel organization of ferrocene moieties replaced the π-stacks of pyrene fragments; ferrocene moieties I and II were stacked above itself. As a result, the major difference in the crystal packing was that each Au-based molecular wire was in a way separate within crystal lattice (Fig. S19 and S24). While the molecular wires stretched in the [100] direction, the 'inter-wire' interactions in the [010] and [001] directions were such that the C–H groups from the Cp rings of one wire tended to point in-between the Cp rings of the adjacent wire (Fig. S19). The wires organize in a way that preserved the bands of the $Au(PEt_3)_2$ groups interspersed with the bands of the pyrene moieties in the **ab** planes.

Table S2. The summary of crystal data and data processing statistics.

Compound	**2b**	**1b'**	**2a**	**1a'**	**1a**
Empirical formula	$C_{18}H_{24}AuFeP$	$C_{38}H_{48}Au_2Fe_2O_2P_2$	$C_{24}H_{24}AuP$	$C_{50}H_{48}Au_2O_2P_2$	$C_{25}H_{24}AuOP$
Formula weight	524.16	1104.33	540.37	1136.75	568.38
Crystal system	orthorhombic	triclinic	monoclinic	triclinic	monoclinic
Space group	P b c a	P -1	C 2/c	P -1	P 21/c
a/Å	13.8716(13)	6.8108(3)	22.426(2)	9.97212(8)	13.69972(11)
b/Å	11.6050(11)	10.4039(4)	9.0304(8)	13.96926(13)	8.58706(6)
c/Å	22.120(2)	27.3603(11)	19.1951(18)	32.1775(2)	18.66191(14)
α/°	90	90.7480(10)	90	86.4576(6)	90
β/°	90	96.5320(10)	99.254(2)	81.5703(6)	107.1539(9)
γ/°	90	106.5310(10)	90	69.9495(8)	90
Volume/$Å^3$	3560.9(6)	1844.42(13)	3836.7(6)	4164.94(6)	2097.73(3)
Z	8	2	8	4	4
μ/mm^{-1}	9.126	8.819	7.757	7.154	7.102
Max. transmission	0.5938	0.7459	0.6988	0.781	1
Min. transmission	0.4088	0.6467	0.2697	0.381	0.37155
Absorption correction	numerical	multi-scan	multi-scan	gaussian	multi-scan
Crystal color	clear dark orange	orange	clear yellow	clear light yellow	clear orange
$\rho_{calc}mg/mm^3$	1.955	1.988	1.871	1.813	1.8
Crystal habit	prism	plate	plate	block	plate
F(000)	2016	1064	2096	2208	1104

Crystal size/mm	0.169	0.303	0.29	0.219	0.33
	0.139	0.078	0.22	0.123	0.27
	0.13	0.04	0.08	0.109	0.05
Rint	0.0354	0.0326	0.0286	0.025	0.0465
Rsigma	0.0182	0.0205	0.014	0.0205	0.0204
Index ranges h	-18:18	-9:9	-31:31	-14:14	-19:19
k	-15:15	-14:14	-12:12	-19:19	-12:12
l	-29:29	-37:37	-26:26	-45:45	-26:26
Reflections collected	44771	67134	51290	99159	68786
2Θ range for data collection	1.84 - 28.86	0.75 - 29.277	1.84 - 30	1.92 - 30	2.28 – 29.99
Temperature/K	100.00(10)	90.00(10)	100.00(10)	100.00(10)	100.00(10)
X-ray wavelength/Å	0.71073	0.71073	0.71073	0.71072	0.71072
Independent reflections I > 2 σ(I)	4136	9003	5329	22638	5498
Independent reflections	4665	9859	5588	24186	6126
Largest diff. peak/hole /e Å^{-3}	1.21 / -0.755	3.603 / -2.57	0.804 / -0.664	2.655 / -1.448	2.404 / -1.013
Goodness-of-fit on F^2	1.032	1.304	1.095	1.171	1.064
Parameters	193	421	238	1017	256
Data	4665	9859	5588	24186	6126

Restraints	0	0	0	0	0
R1 all data	0.0207	0.03	0.0142	0.0231	0.0243
R1 [I>=2σ (I)]	0.0159	0.0257	0.0131	0.0206	0.02
wR2 [I>=2σ (I)]	0.0326	0.0632	0.03	0.0428	0.0478
wR2 all data	0.0339	0.0714	0.0304	0.0436	0.0499

Table S3. Selected bond lengths for described compounds in Å.

	2a	**1a'**				**1a**	**2b**	**1b'**	
		I	II	III	IV			I	II
Au–P	2.2816(5)	2.3105(7)	2.3124(7)	2.3057(7)	2.3078(7)	2.2780(8)	2.2764(6)	2.312(1)	2.313(1)
Au–C	2.006(2)	1.985(3)	1.977(3)	1.984(3)	1.986(3)	2.001(3)	1.995(2)	1.990(4)	1.992(4)
C≡C	1.211(2)	1.207(3)	1.215(3)	1.212(3)	1.215(3)	1.210(4)	1.206(3)	1.211(6)	1.210(6)
$C_{C=O}$–$C_{C≡C}$		1.446(3)	1.450(3)	1.454(3)	1.449(3)	1.449(4)		1.448(6)	1.447(6)
C=O		1.232(4)	1.228(3)	1.230(3)	1.228(3)	1.228(3)		1.234(5)	1.229(5)
C–L	1.439(2)	1.487(4)	1.492(4)	1.492(4)	1.492(4)	1.490(4)	1.432(3)	1.465(6)	1.468(6)
P–Cp_1 plane	0.112(4)						0.341(3)		
Au–Cp_1 plane	0.181(4)	0.916(3)	0.734(3)	0.636(3)	1.181(3)		0.093(3)		

Table S4. Selected interatomic angles for described compounds in °.

Valence Angles	**2a**	**1a'**				**1a**	**2b**	**1b'**	
		I	II	III	IV			I	II
P–Au–C	176.61(5)					177.59(8)	176.48(7)		
Au–C≡C	174.1(2)	176.7(4)	174(4)	175.2(4)	177.1(4)	178.4(2)	175.1(2)	177.5(4)	176.1(4)
C≡C–C	176.8(2)	175.0(3)	177.9(3)	177.8(3)	174.5(3)	177.7(3)	178.0(2)	177.7(4)	176.7(4)
Dihedral Angles									
O–C–C–L		13.1(4)	161.6(3)	-160.1(3)	-19.0(4)	17.6(4)		-177.3(4)	-11.9(6)
$C_{C\equiv C}$–$C_{C=O}$–C–L		11.0(4)	166.4(2)	-166.3(2)	-18.8(4)	18.0(3)		2.3(6)	2.1(3)
C_{Et}–P–C–L	174.8(1)					-14.8(2)	-5.8(2)		
C16–P1–Au2–Au1		12.73	171.33	37.3	162.47			20.6(2)	29.6(2)
O–$C_{C\equiv C}$ … $C_{C\equiv C}$–O		-173.3(3)		-178.4(3)					

Table S5. Selected geometric parameters describing aurophilic interactions for **1a'**, **1b'** and **2a** in Å/°.

	1a'				**1b'**		**2a**
Distances							
# of Au atom	1 – 2	2 – 3	3 – 4	4 … 1	1 – 2		
Au … Au	3.1468(6)	3.2446(6)	3.0396(6)	4.566(5)	3.2347(3)		3.1887(6)
# of pyrene moiety	1 – 1	2 – 2	3 – 3	4 – 4			
pyr … pyr	3.387(4)	3.400(4)	3.369(5)	3.414(4)			
Valence Angles							
					I	II	
Au–Au–C	90.95(4)	91.15(3)	94.22(4)	84.49(4)	102.7(1)	76.4(1)	83.36(5)
Au–Au–P	94.72(4)	84.35(3)	93.89(4)	98.19(3)	92.25(3)	90.42(3)	99.56(2)
P–Au–P	178.08(4)		167.92(4)		177.31(4)		
C–Au–C	175.9(4)		177.3(4)		179.0(2)		
Au–Au–Au	175.76(4)	174.22(4)	177.07(4)	171.73(4)	175.79(1)		
Dihedral Angles							
P–Au–Au–P							89.87(2)
C–Au–Au–P	82.67(5)	85.57(4)	72.48(5)	70.62(5)	76.6(1)		

Table S6. Selected geometric parameters describing ferrocene moieties - distances in Å, torsion angles in °.

	1b	**1b'**	
		I	II
Fe … Cp1	1.639(6)	1.643(5)	1.649(5)
Fe … Cp2	1.648(6)	1.649(5)	1.643(5)
Cp1 plane … Cp2 plane	3.16(5)	0.71(6)	0.66(6)
Cp1_I … Cp1_II		1.63(4)	
C1–Cp1–Cp2–C6	-9.6(5)	-2.22(7)	1.64(7)

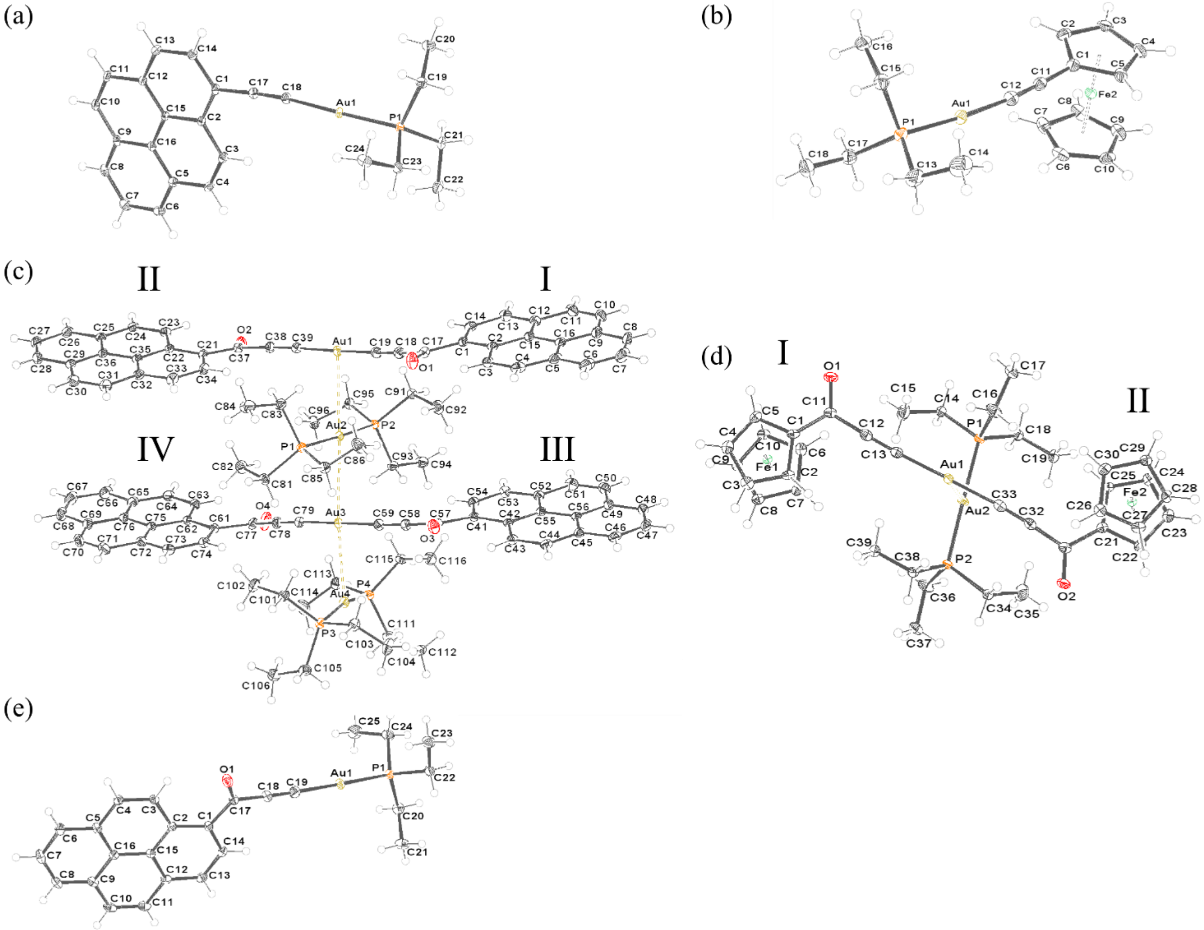

Fig. S17. The ORTEP representation of compounds (a) **2a**, (b) **2b**, (c) **1a'**, (d) **1b'** and (e) **1a** with labelling scheme. Atomic displacement parameters represented at 50% probability level. Hydrogen atom numbers are the same as the numbers of connected C atoms

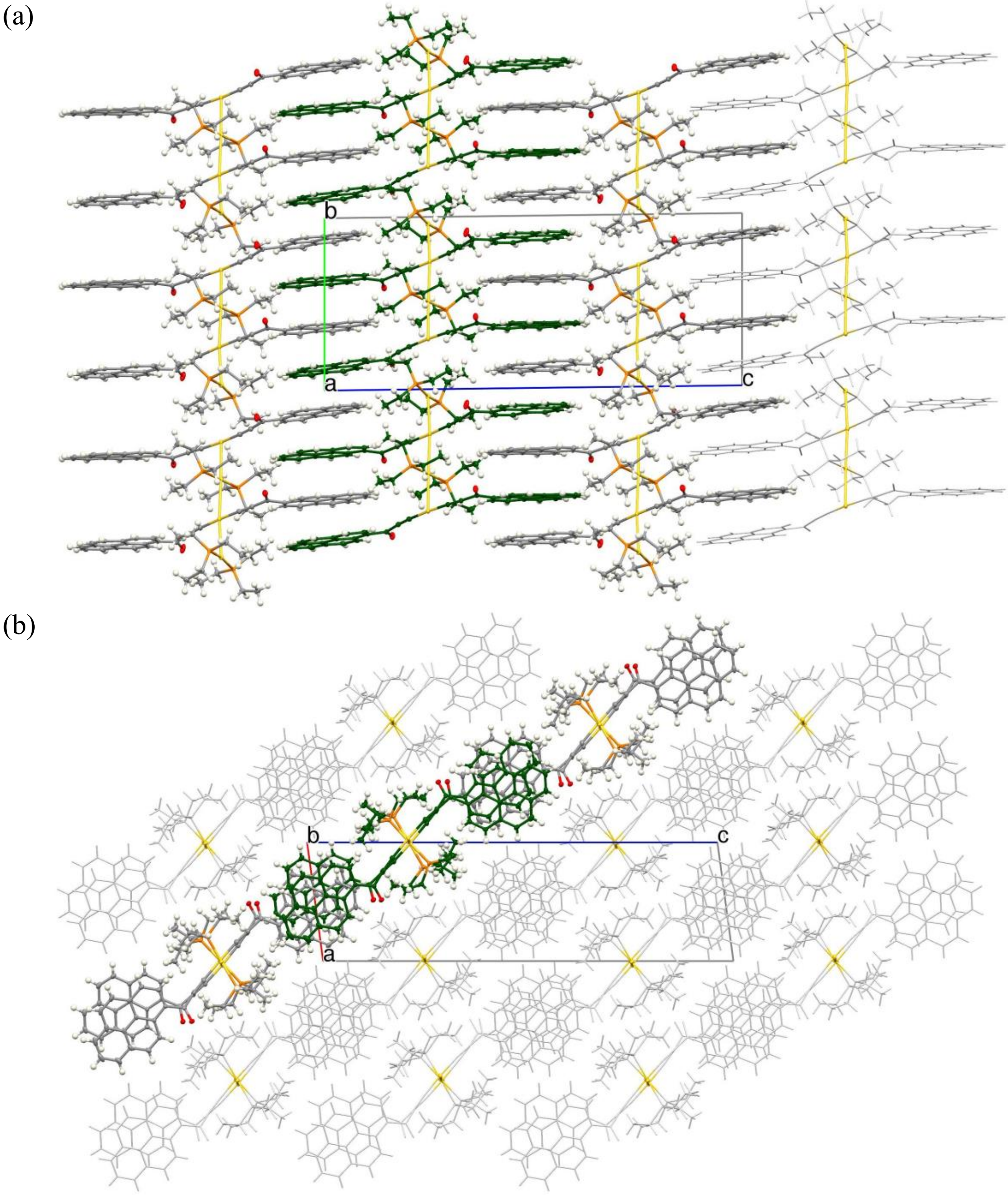

Fig. S18. Crystal packing of **1a'** in the a (a) and the b (b) crystallographic direction. A central set of molecular sticks enhanced by atomic displacement ellipsoid representation (ADP-s at 50% probability level) and green carbon atoms. The series of adjacent π-stacked molecular sticks, forming layer in the [-101] direction is also enhanced, remaining molecules (apart from Au atoms) represented as grey sticks for clarity

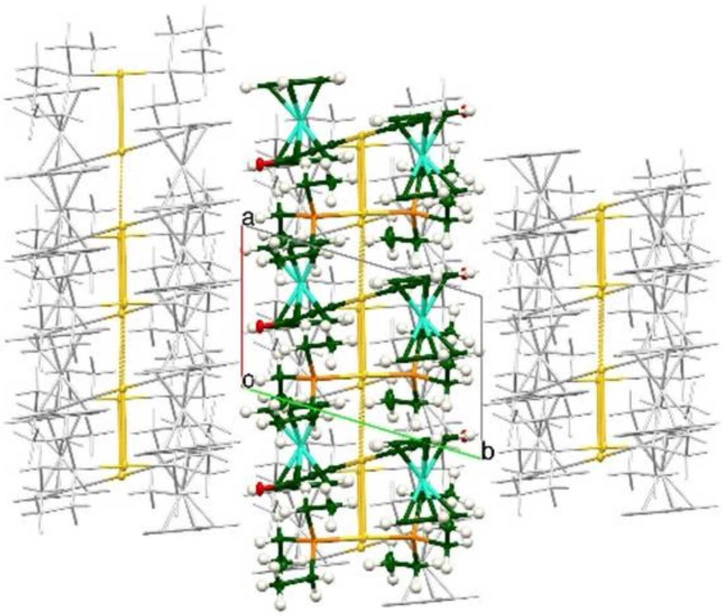

Fig. S19. Crystal packing of **1b'** in the [001] crystallographic direction. A central molecular wire motif enhanced by atomic displacement ellipsoid representation (ADP-s at 50% probability level) and green carbon atoms. The remaining molecules (apart from Au atoms) represented as grey sticks for clarity.

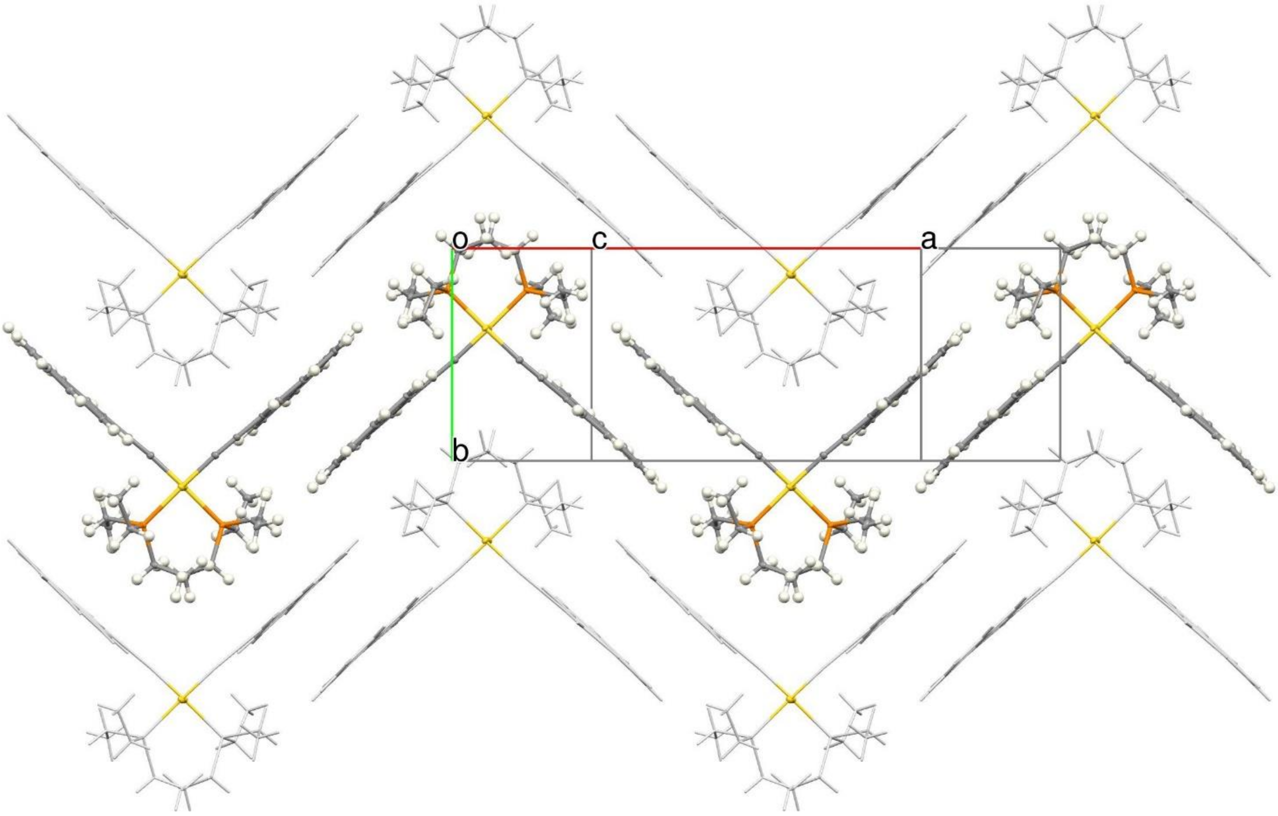

Fig. S20. View of the **2a** dimers exactly along the Au … Au interaction. A ribbon of π-stacked dimers is enhanced (ellipsoid representation, ADP-s at 50% probability level)within a layer of stacked molecules. The remaining molecules (apart from Au atoms) represented as grey sticks for clarity.

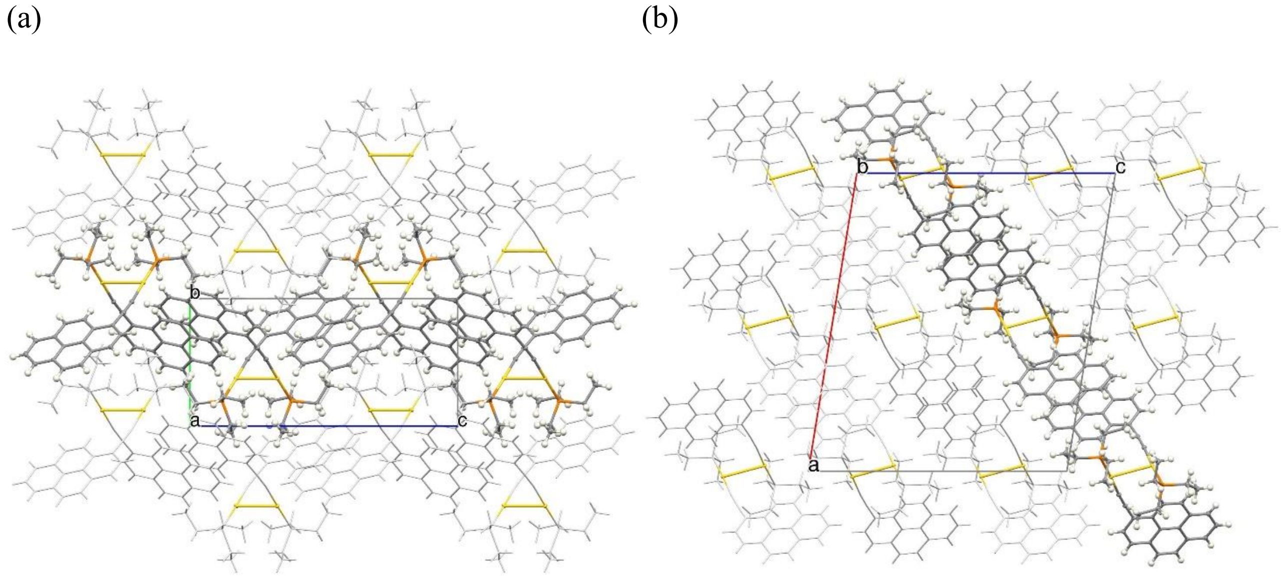

Fig. S21. Crystal packing of **2a** in the **a** (a) and the **b** (b) crystallographic direction. A ribbon of π-stacked dimers is enhanced within the crystallattice by atomic displacement ellipsoid representation (ADP-s at 50% probability level), remaining molecules (apart from Au atoms) represented as grey sticks for clarity.

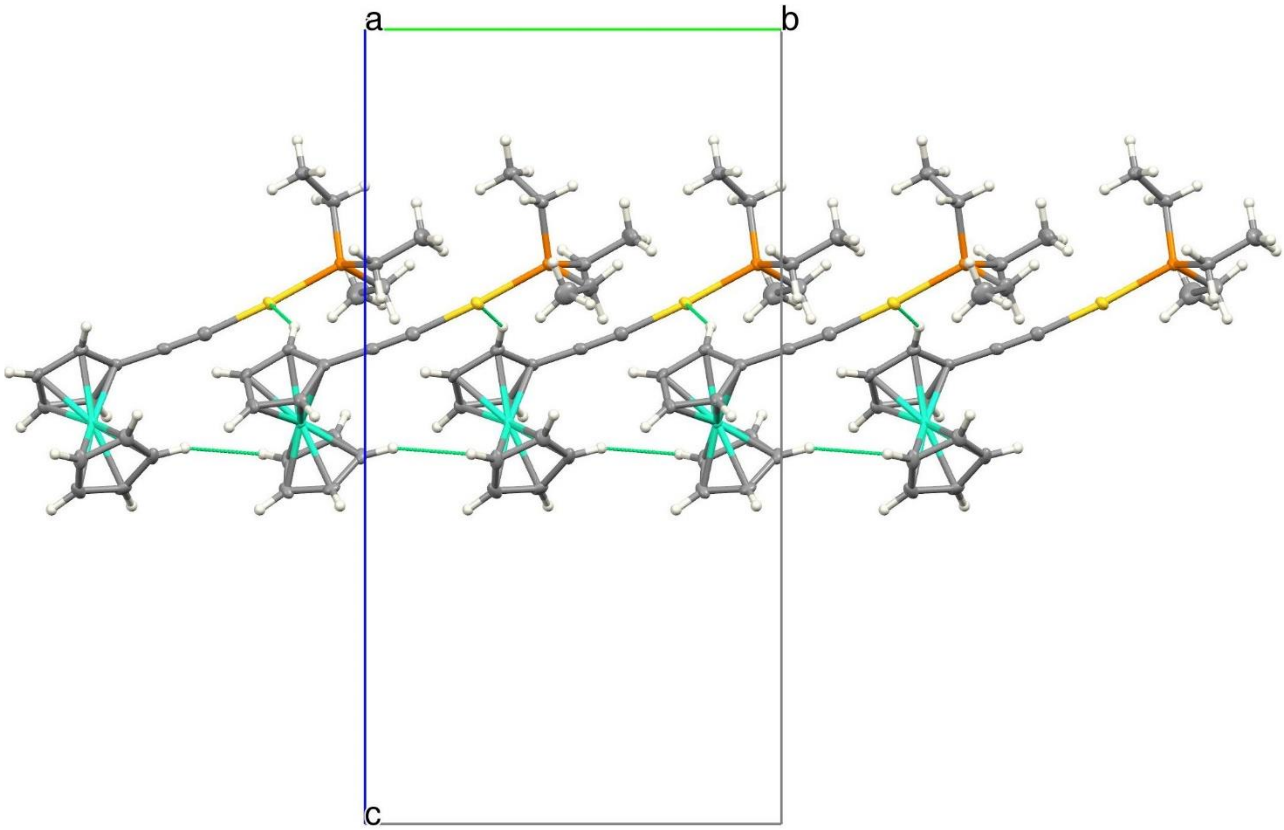

Fig. S22. Basic packing motif in the **2b** structure (ellipsoid representation, ADP-s at 50% probability level). The adjacent ferrocene moieties are oriented perpendicularly. The shortest Au … H and H … H contacts showed in green.

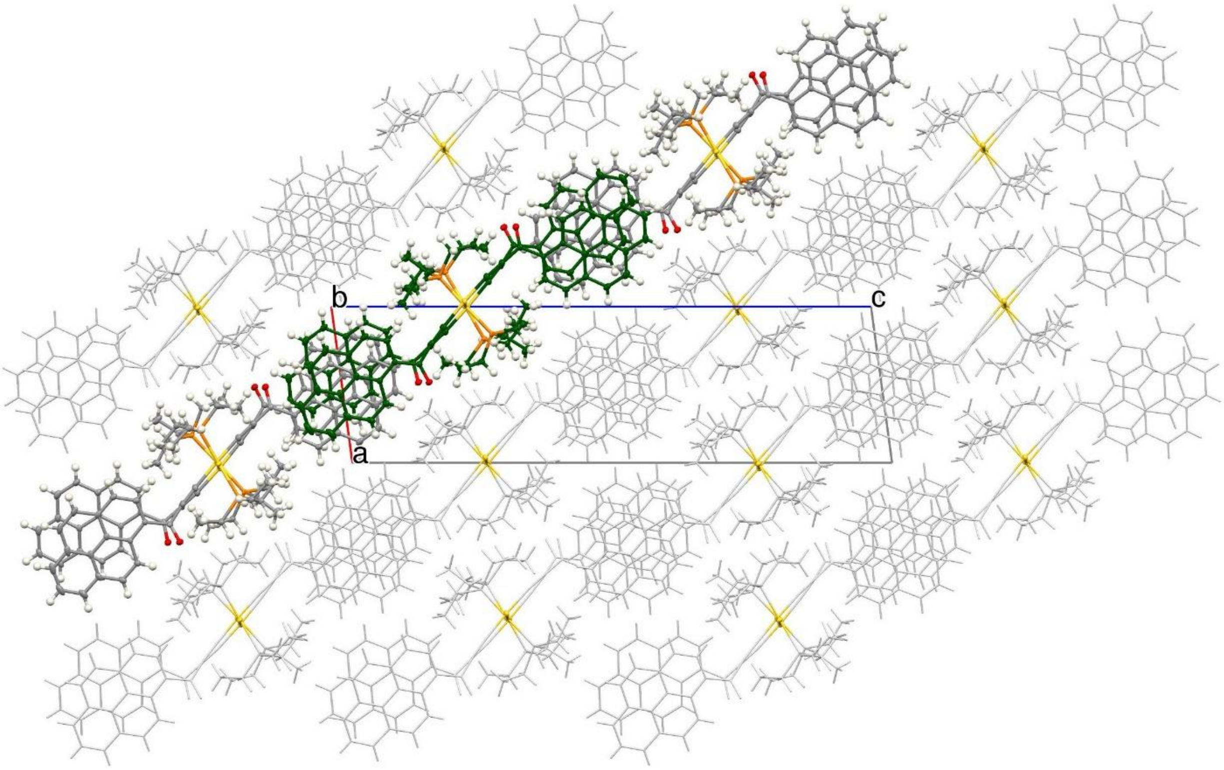

Fig. S23. Crystal packing of **1a'** in the **b** crystallographic direction. A central set of molecular sticks enhanced by atomic displacement ellipsoid representation (ADP-s at 50% probability level) and green carbon atoms. The series of adjacent π-stacked molecular sticks, forming layer in the [-101] direction is also enhanced, remaining molecules (apart from Au atoms) represented as grey sticks for clarity.

(a)

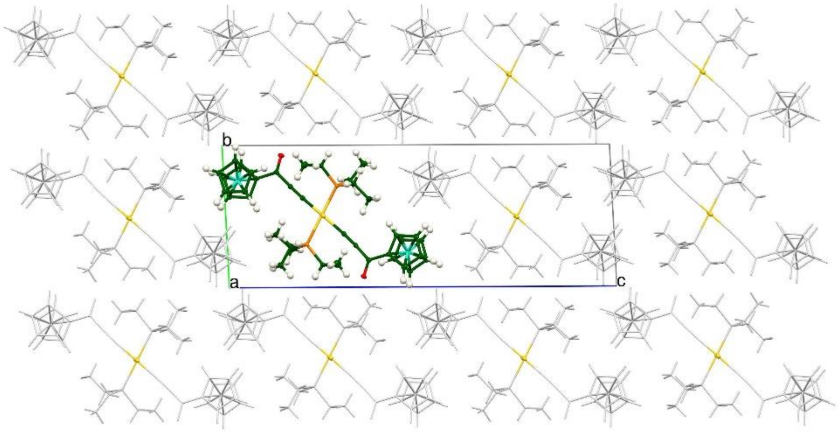

Fig. S24. Crystal packing of **1b'** in the **c** crystallographic direction. A central molecular wire motif enhanced by atomic displacement ellipsoid representation (ADP-s at 50% probability level) and green carbon atoms. The remaining molecules (apart from Au atoms) represented as grey sticks for clarity.

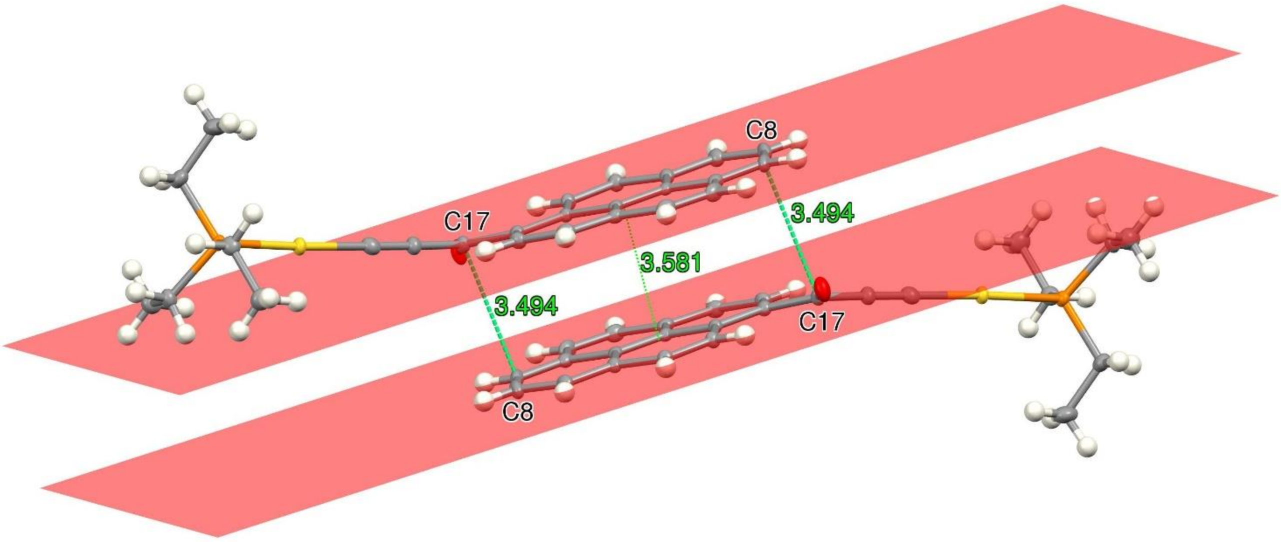

Fig. S25. Basic packing motif in **1a** structure (ellipsoid representation, ADP-s at 50% probability level) showing parallel pyrene planes of molecules related by crystallographic center of inversion. The shortest C … C and the average distance between pyrene planes showed in green. Measurements in Å.

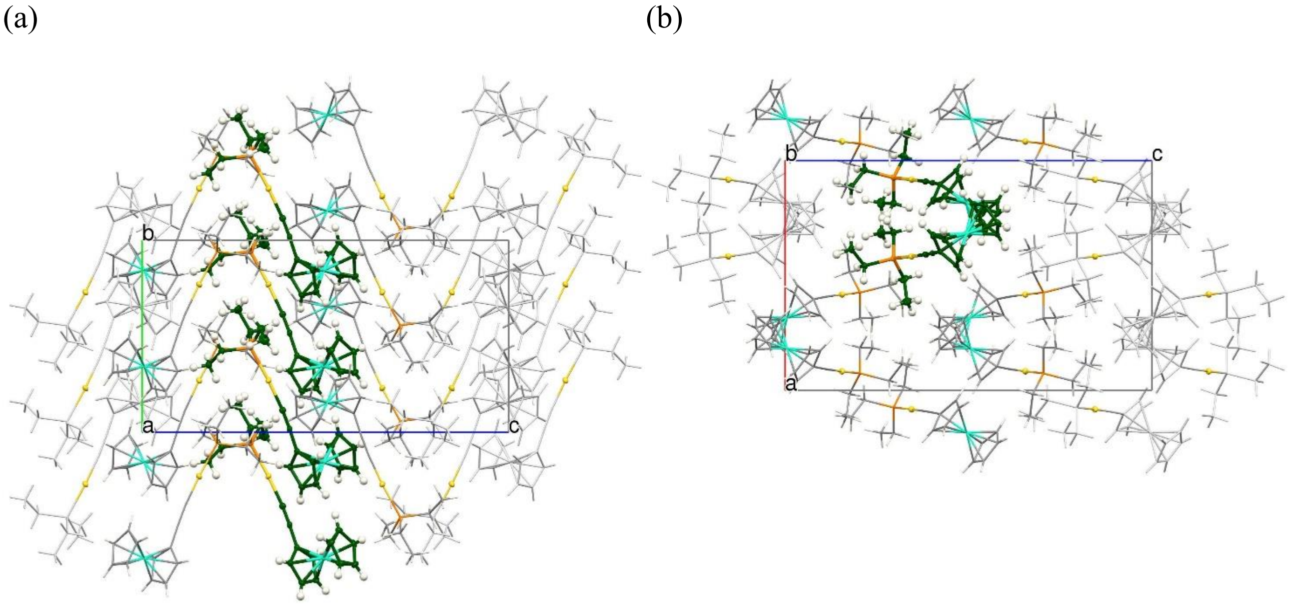

Fig. S26. Crystal packing of **2b** in the **a** (a) and the **b** (b) crystallographic direction. A ribbon of parallel oriented 1b molecules is enhanced by atomic displacement ellipsoid representation (ADP-s at 50% probability level) and green carbon atoms. Adjacent ribbons of **2b** represented as sticks but colored by element, remaining molecules (apart from Au and Fe atoms) represented as grey sticks for clarity.

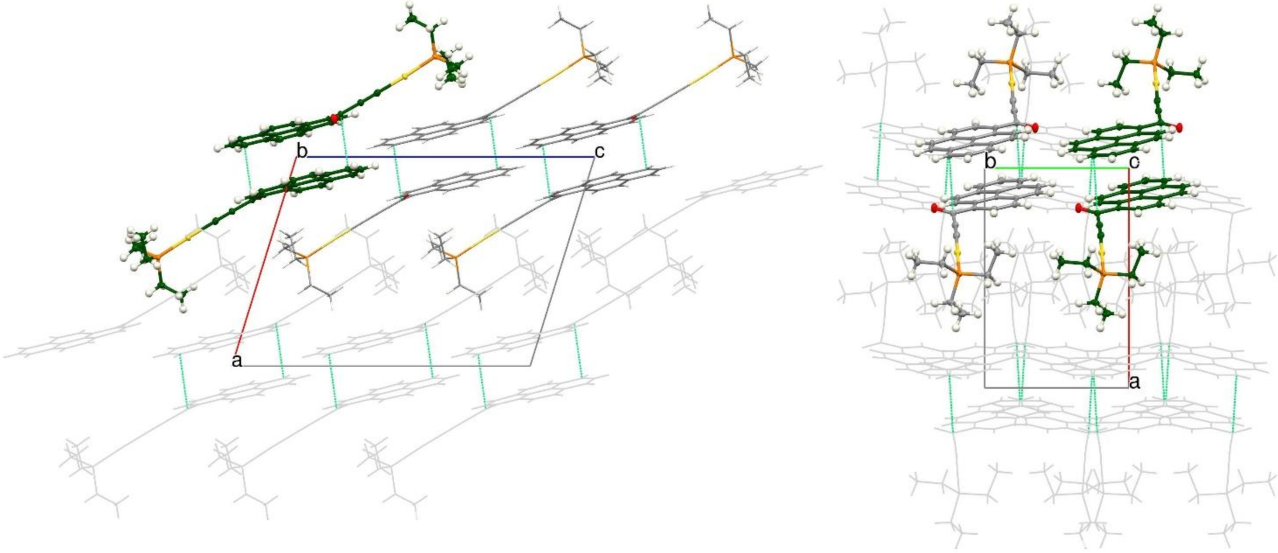

Fig. S27. Crystal packing of **1a** in the **b** (a) and the **c** (b) crystallographic direction. A π-stacked dimer of **1a** enhanced by atomic displacement ellipsoid representation (ADP-s at 50% probability level) and green carbon atoms. The series of adjacent dimers stretching in the **c** and **b** directions also enhanced, remaining molecules (apart from Au and Fe atoms) represented as grey sticks for clarity. The shortest C … C and the average distance between pyrene planes showed in green.

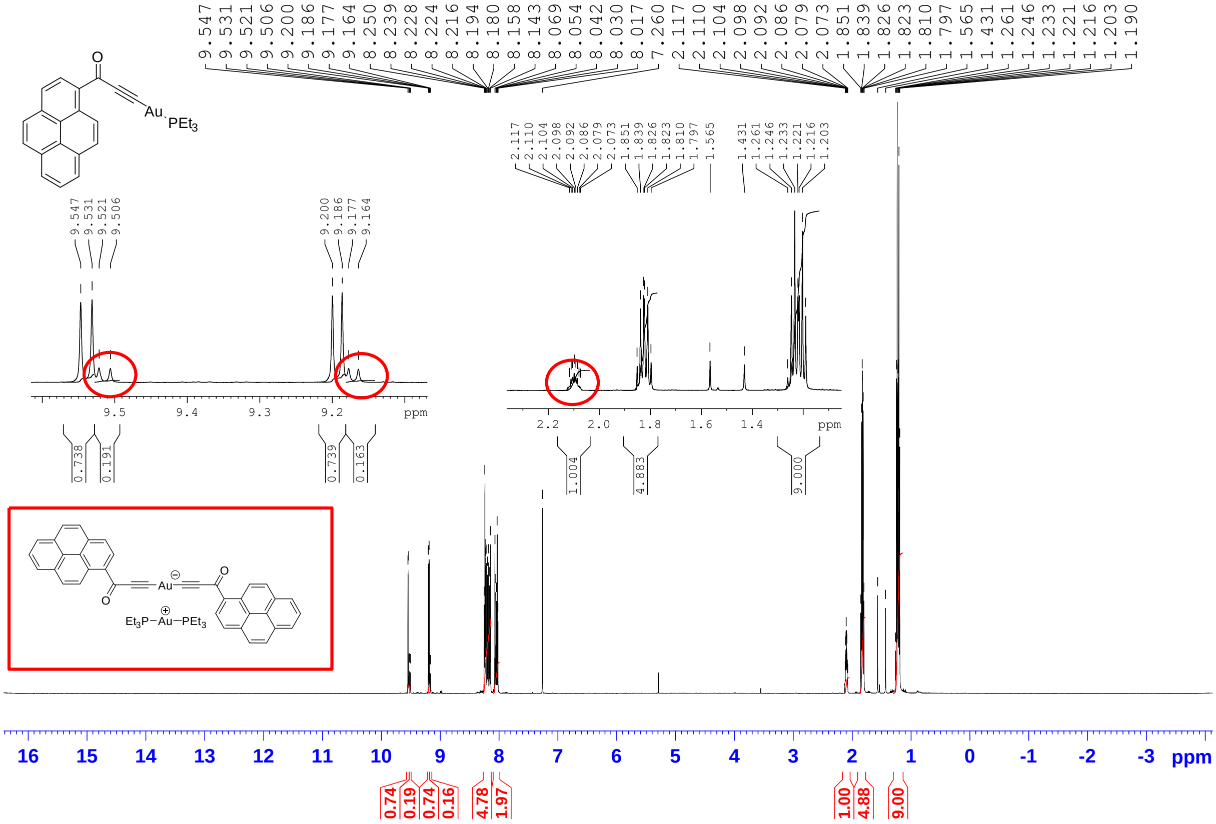

Fig. S28 ^{1}H NMR spectrum of **1a** (CDCl$_3$)

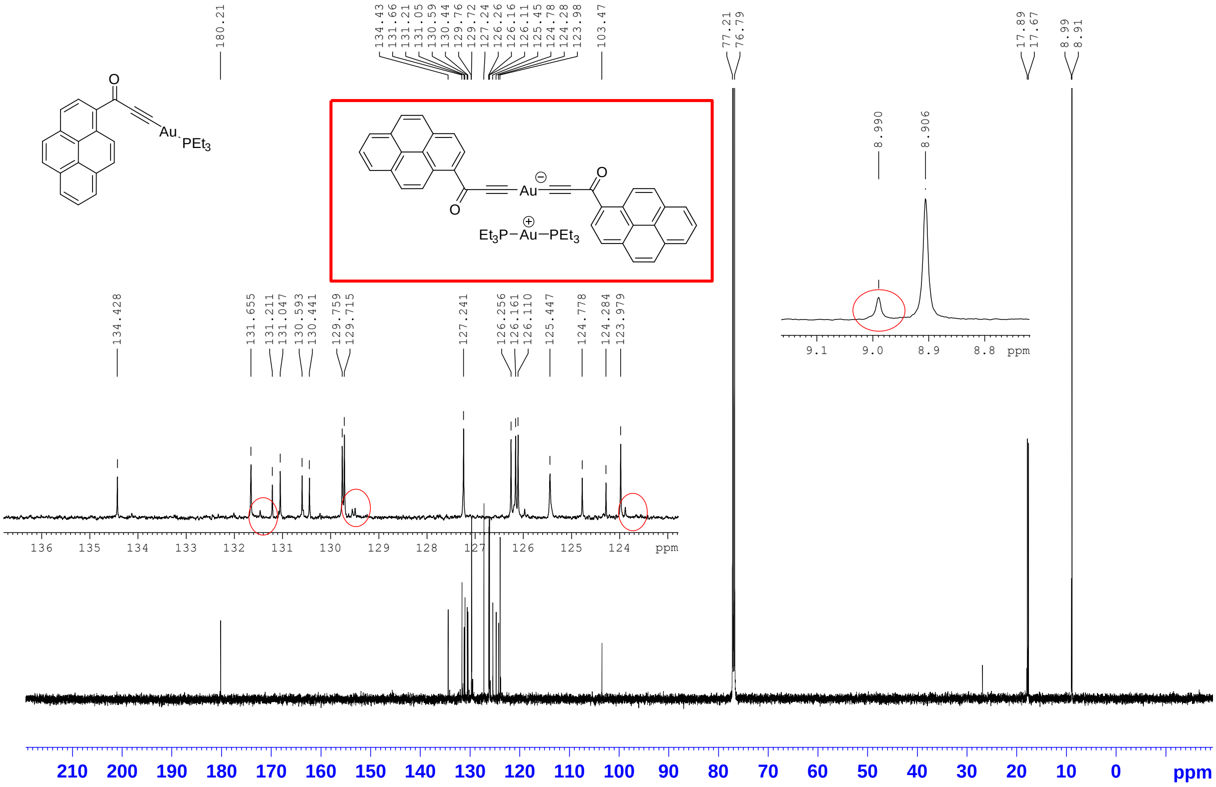

Fig. S29 ^{13}C{^{1}H} NMR spectrum of **1a** (CDCl$_3$)

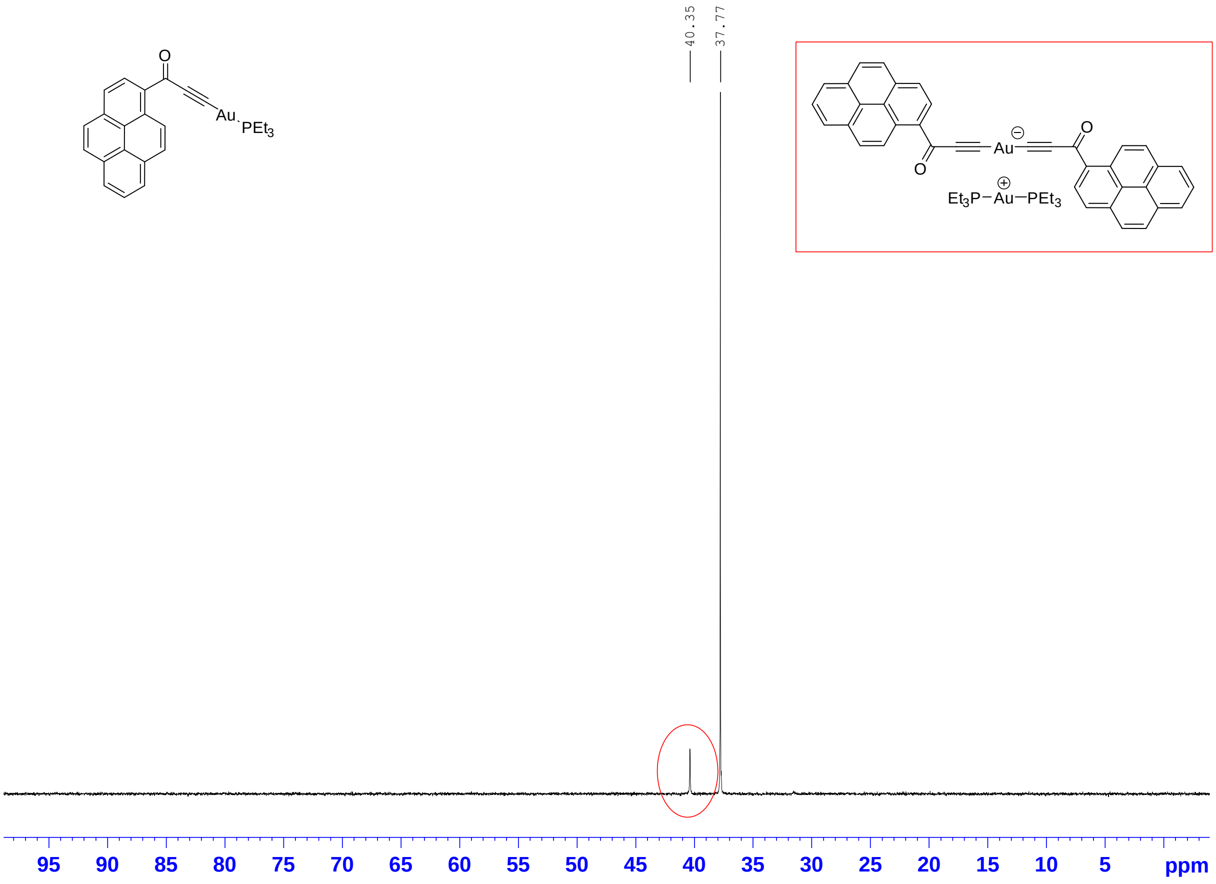

Fig. S30 ^{31}P{^{1}H} NMR spectrum of **1a** ($CDCl_3$)

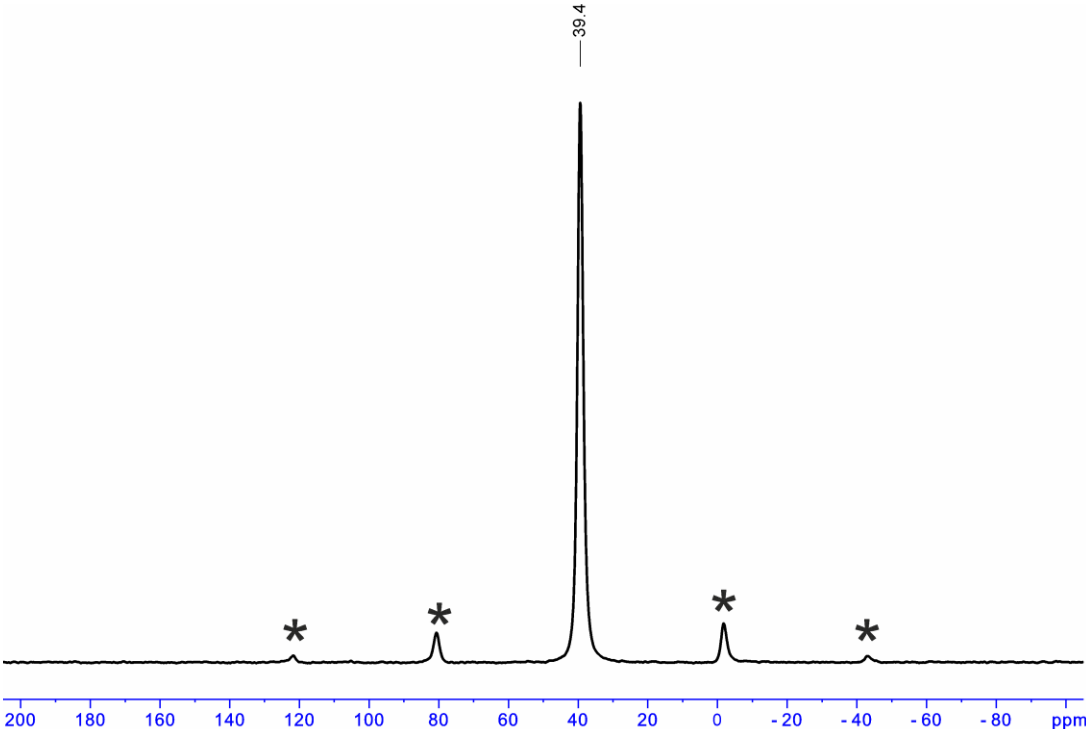

Fig. S31 ^{31}P CP-MAS NMR spectrum of **1a** (solid) recorded at spinning speed equal to 8kHz. Spinning sidebands were marked with asterisk.

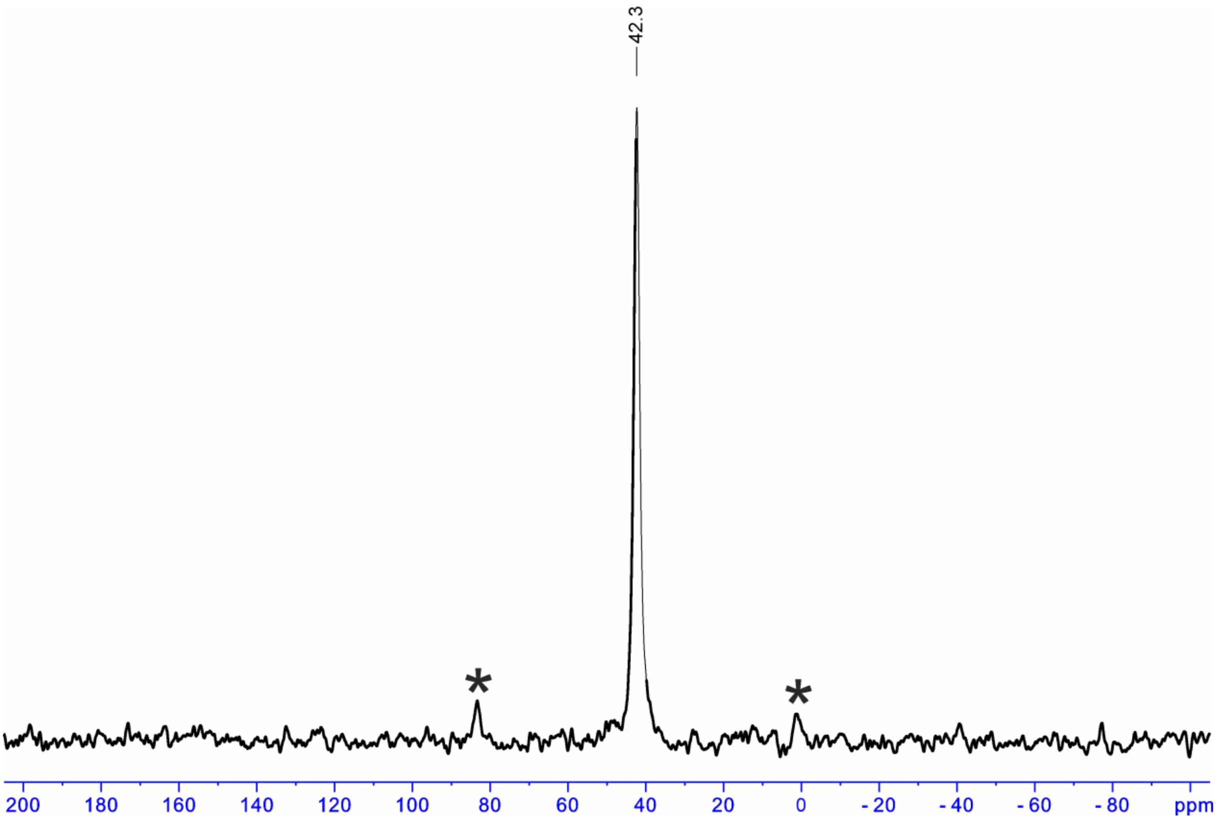

Fig. S32 ^{31}P CP-MAS NMR spectrum of **1a’** (solid) recorded at spinning speed equal to 8kHz. Spinning sidebands were marked with asterisk.

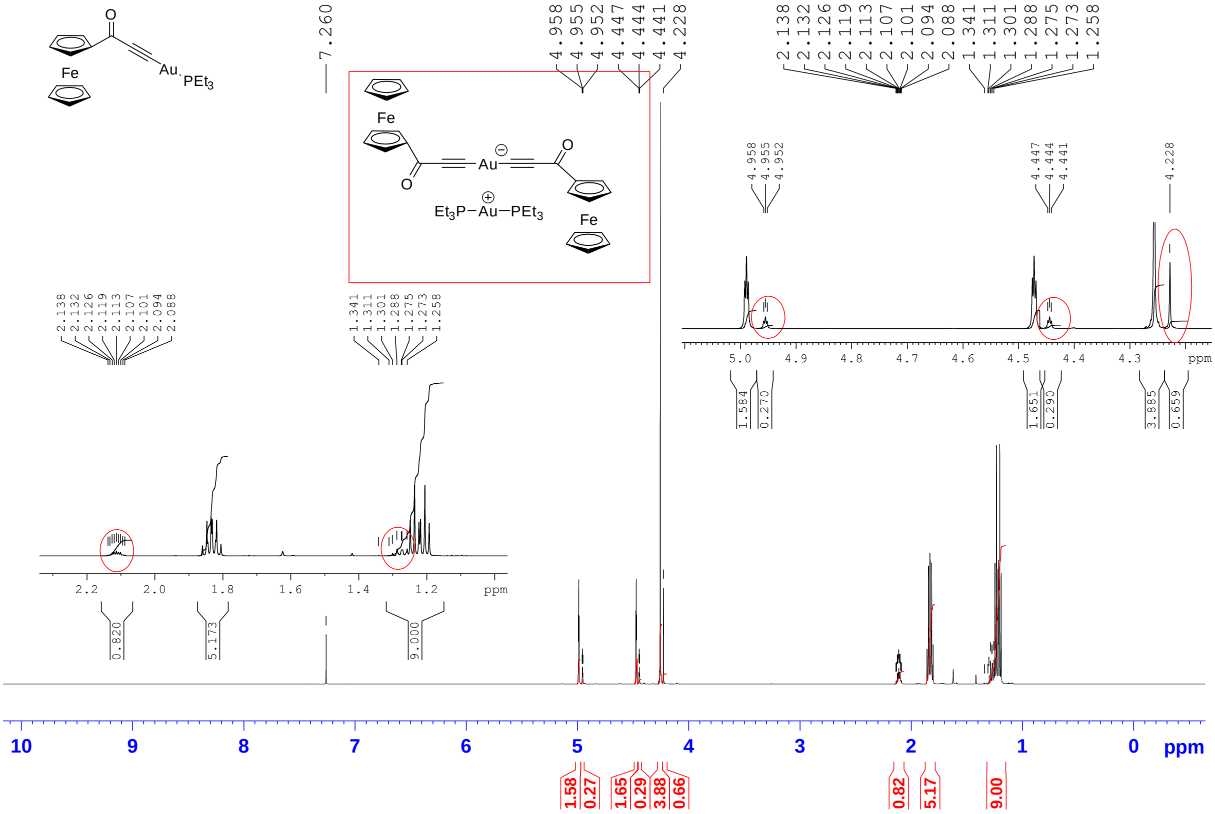

Fig. S33 ^{1}H NMR spectrum of **1b** (CDCl$_3$)

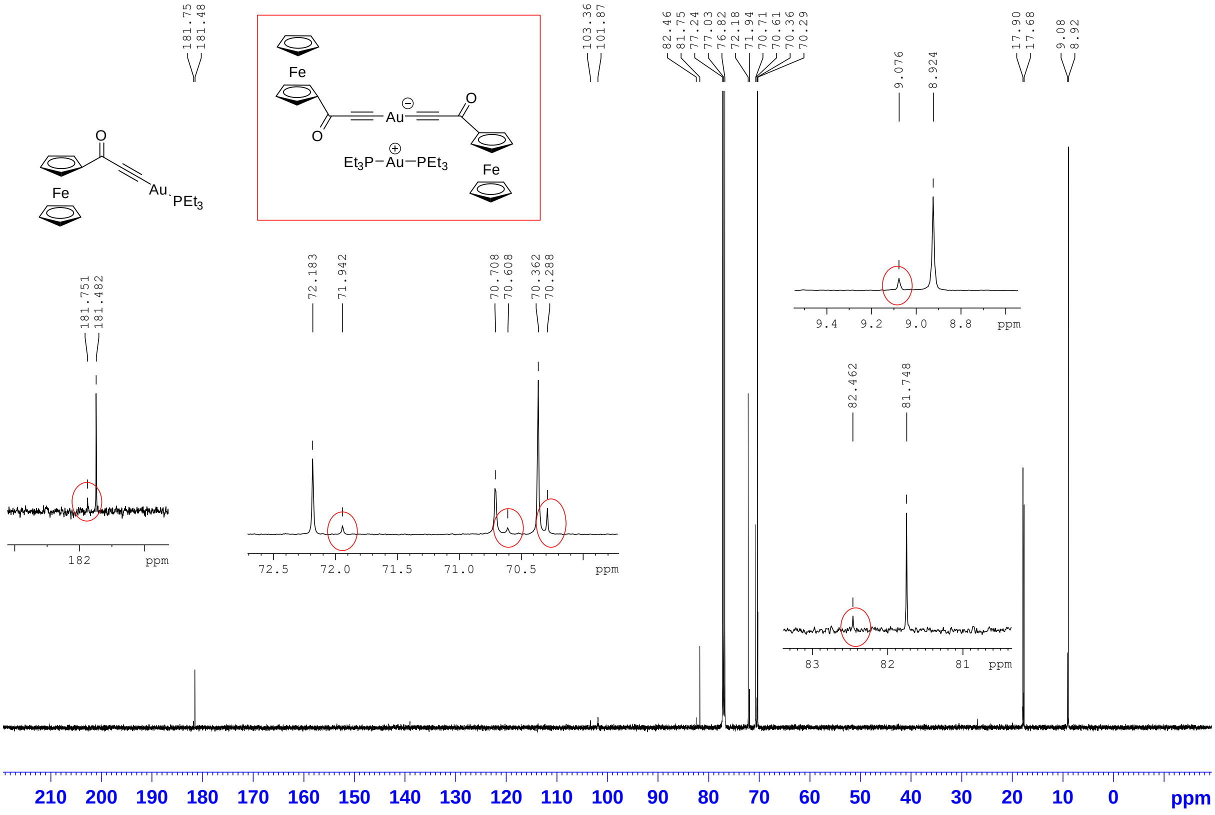

Fig. S34 ^{13}C{^{1}H} NMR spectrum of **1b** (CDCl$_3$)

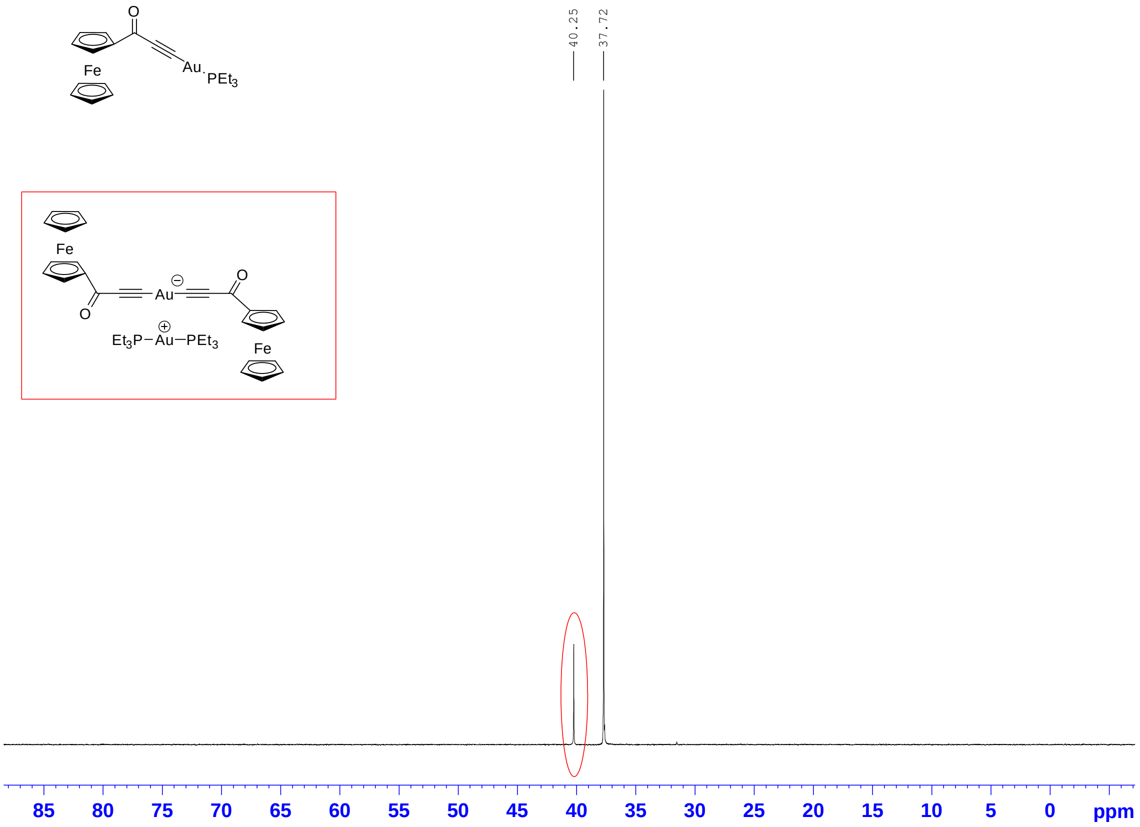

Fig. S35 $^{31}P\{^1H\}$ NMR spectrum of **1b** ($CDCl_3$)

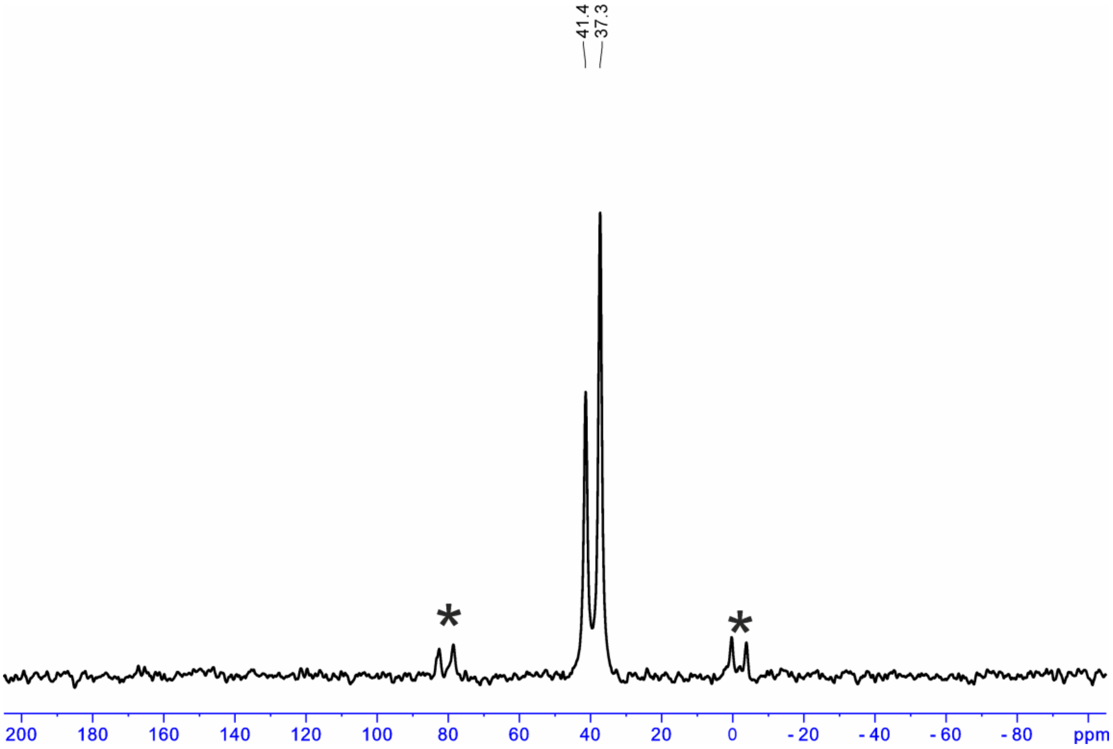

Fig. S36 ^{31}P CP-MAS NMR spectrum of a mixture of **1b** and **1b’** (solid) recorded at spinning speed equal to 8kHz . Spinning sidebands were marked with asterisk.

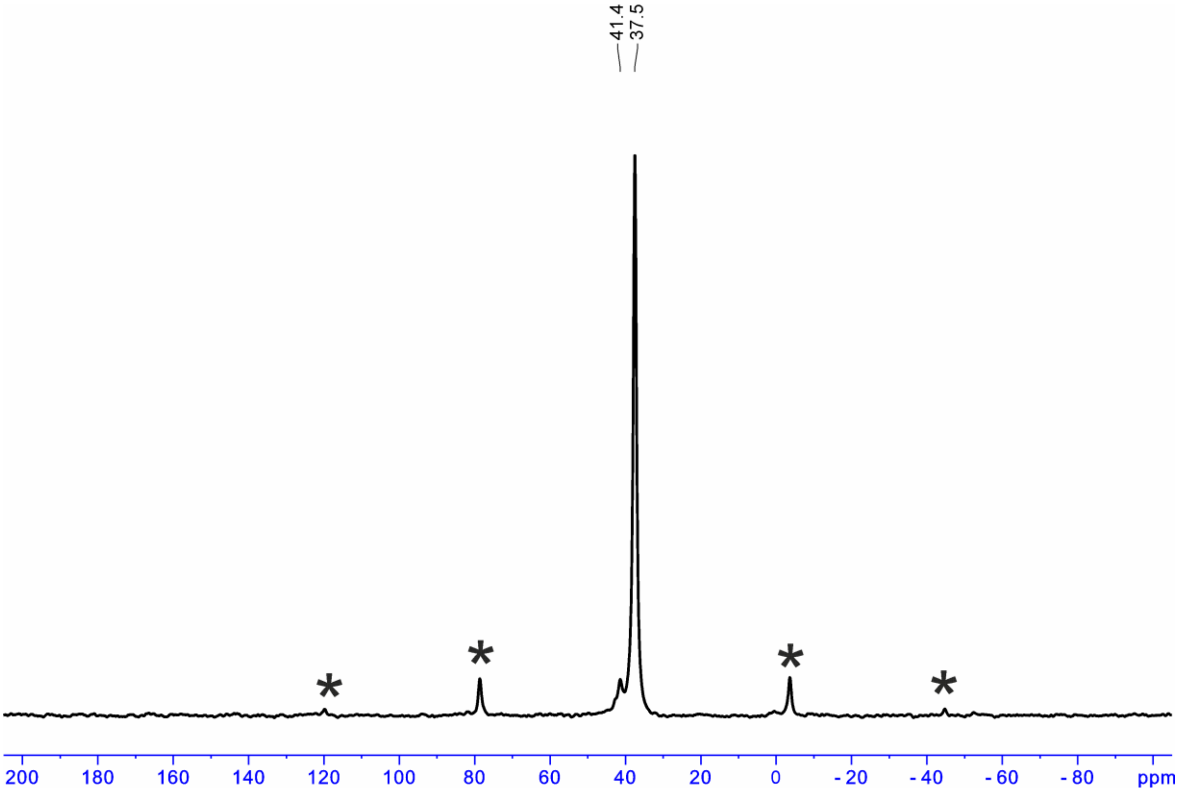

Fig. S37 ^{31}P CP-MAS NMR spectrum of **1b** (solid) recorded at spinning speed equal to 8kHz . Spinning sidebands were marked with asterisk.

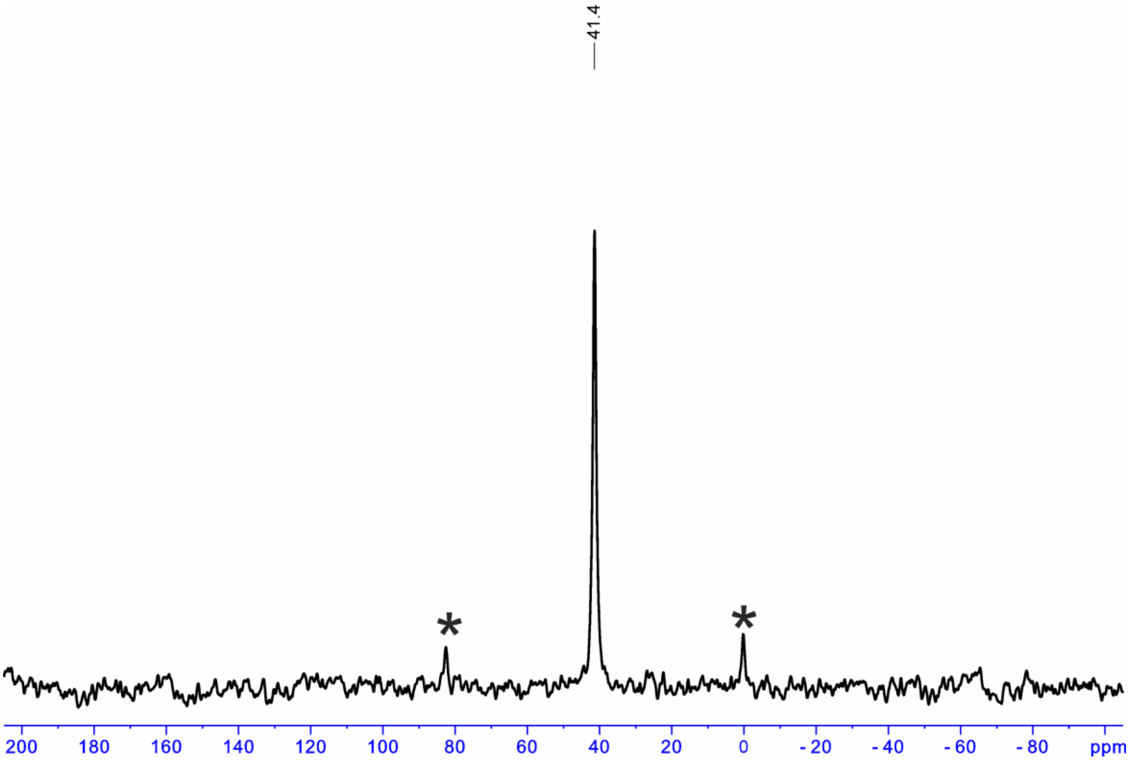

Fig. S38 ^{31}P CP-MAS NMR spectrum of **1b’** (solid) recorded at spinning speed equal to 8kHz. Spinning sidebands were marked with asterisk.

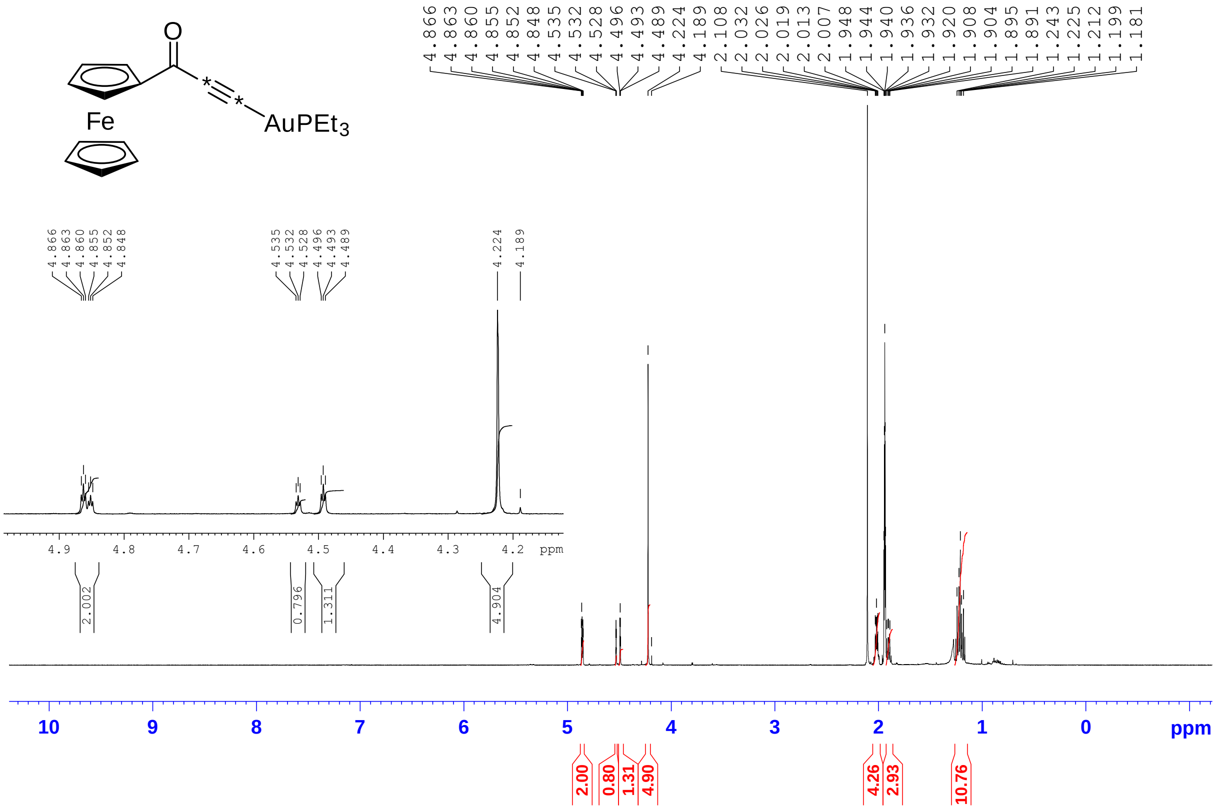

Fig. S39 ^{1}H NMR spectrum of ^{13}C labeled **1b** (CD_3CN)

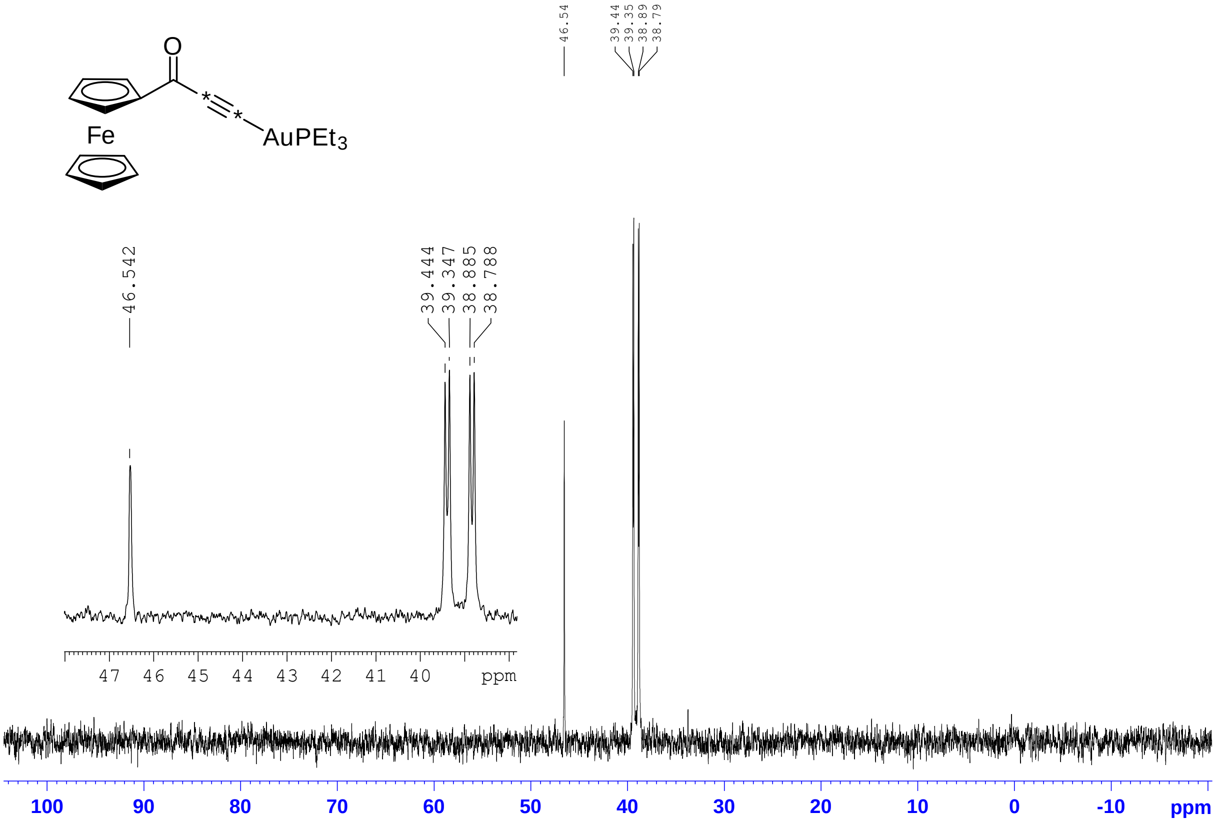

Fig. S40 ^{31}P{^{1}H} NMR spectrum of ^{13}C labeled **1b** (CD_3CN)

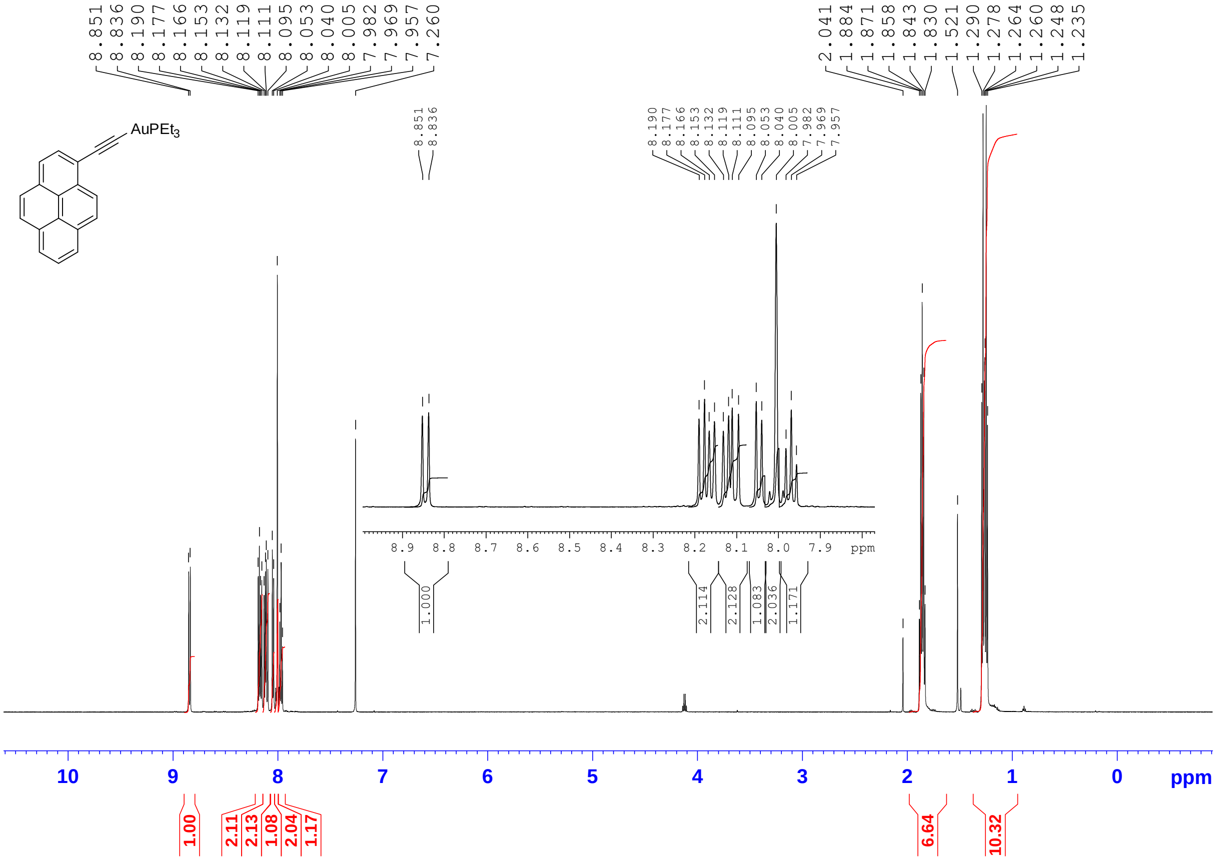

Fig. S41 ^{1}H NMR spectrum of **2a** (CDCl$_3$)

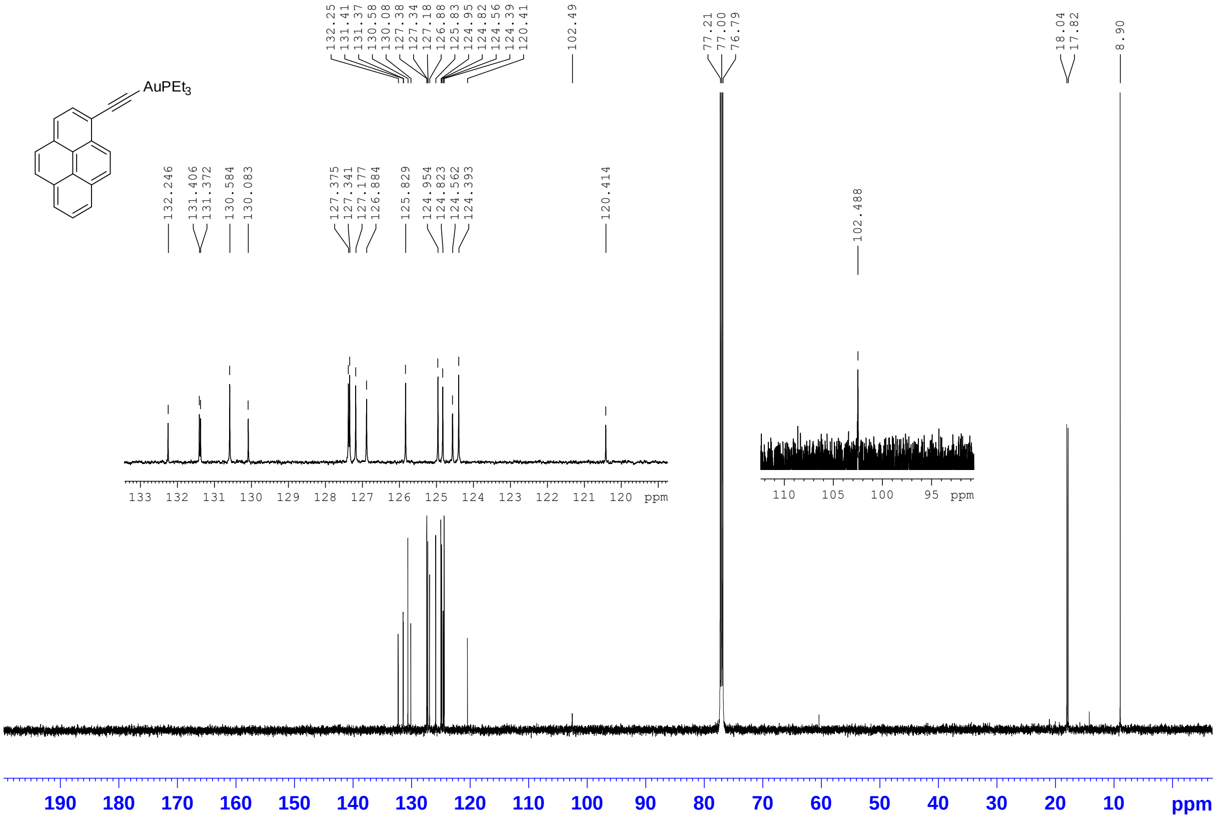

Fig. S42 ^{13}C{^{1}H} NMR spectrum of **2a** (CDCl$_3$)

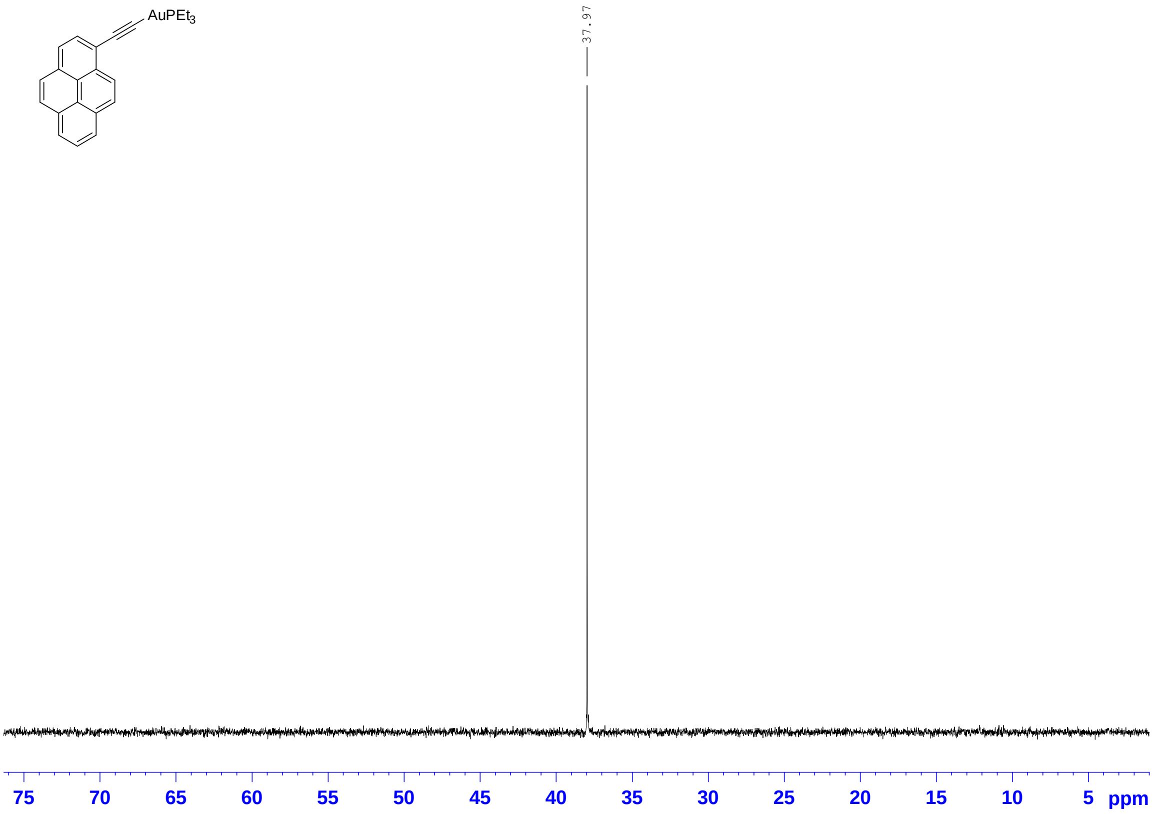

Fig. S43 $^{31}P\{^{1}H\}$ NMR spectrum of **2a** ($CDCl_3$)

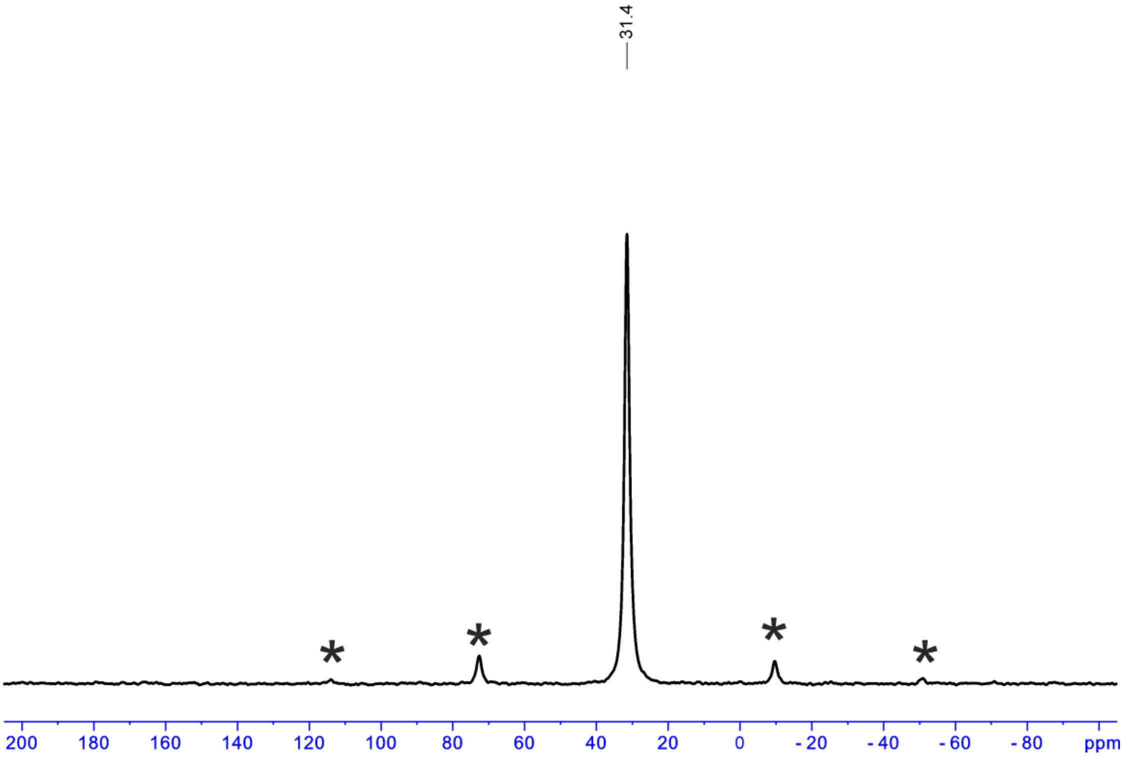

Fig. S44 ^{31}P CP-MAS NMR spectrum of **2a** (solid) recorded at spinning speed equal to 8kHz . Spinning sidebands were marked with asterisk.

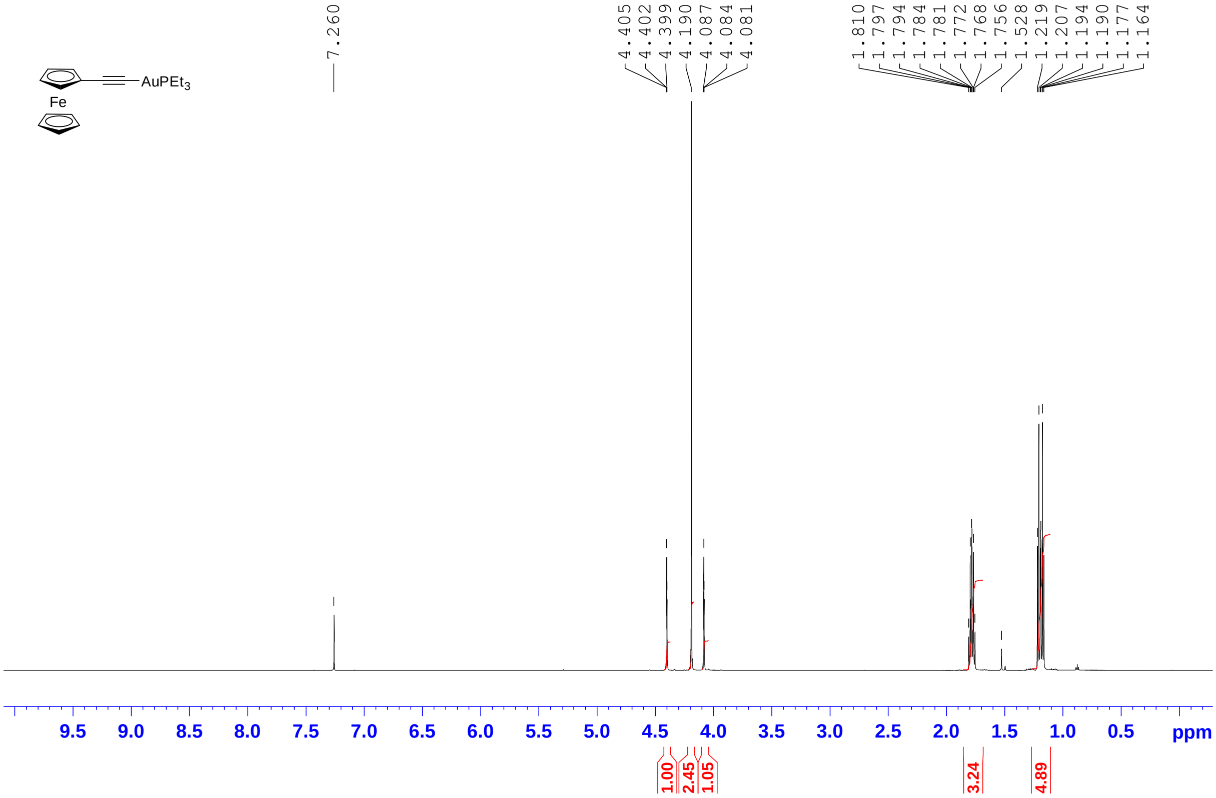

Fig. S45 ^{1}H NMR spectrum of **2b** ($CDCl_3$)

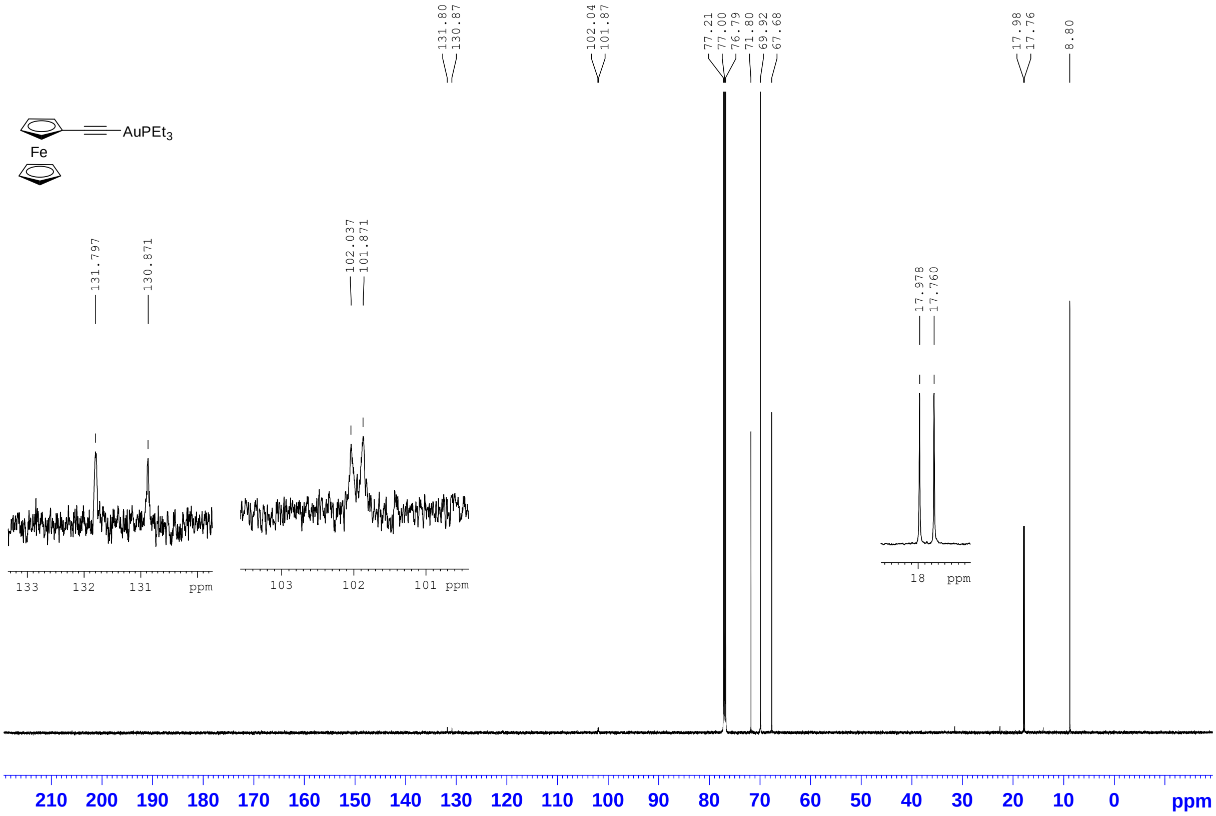

Fig. S46 $^{13}C\{^{1}H\}$ NMR spectrum of **2b** ($CDCl_3$)

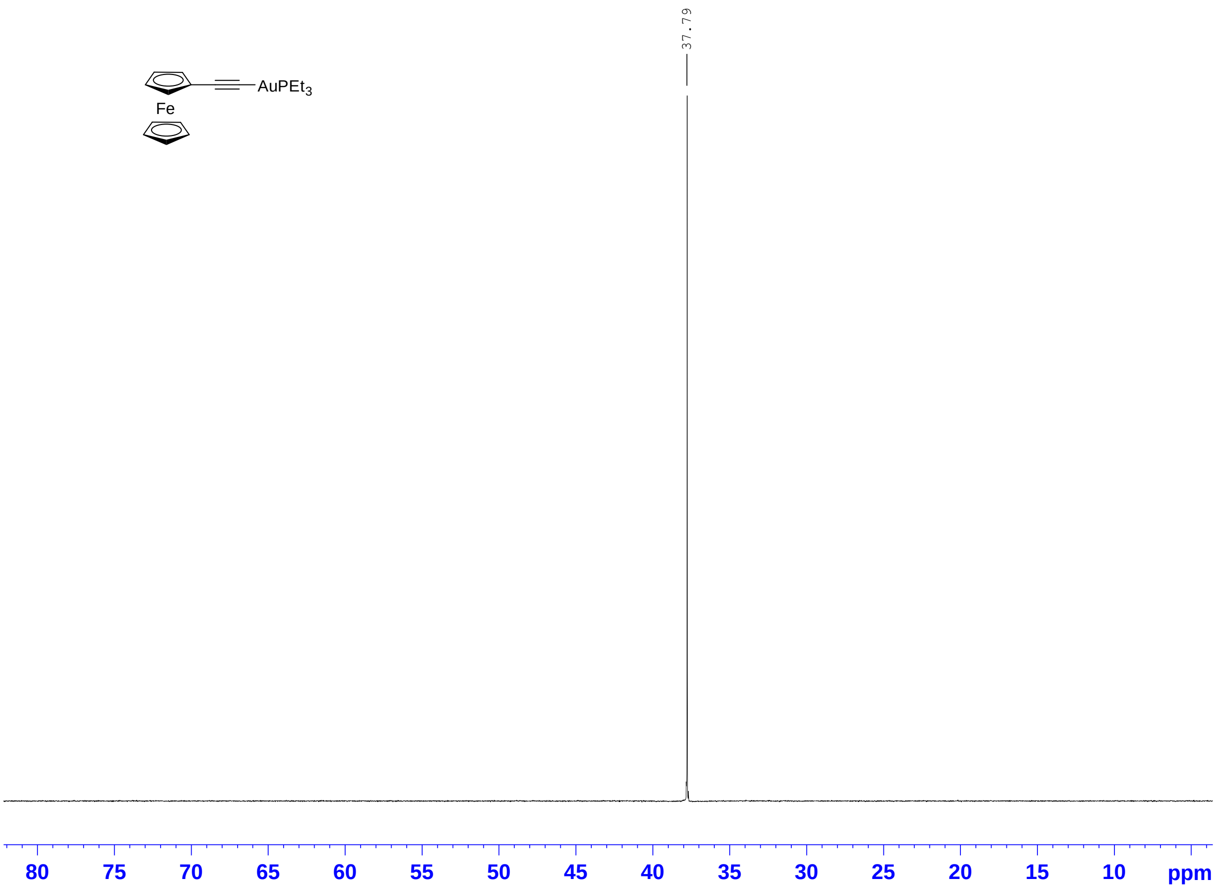

Fig. S47 $^{31}P\{^{1}H\}$ NMR spectrum of **2b** ($CDCl_3$)

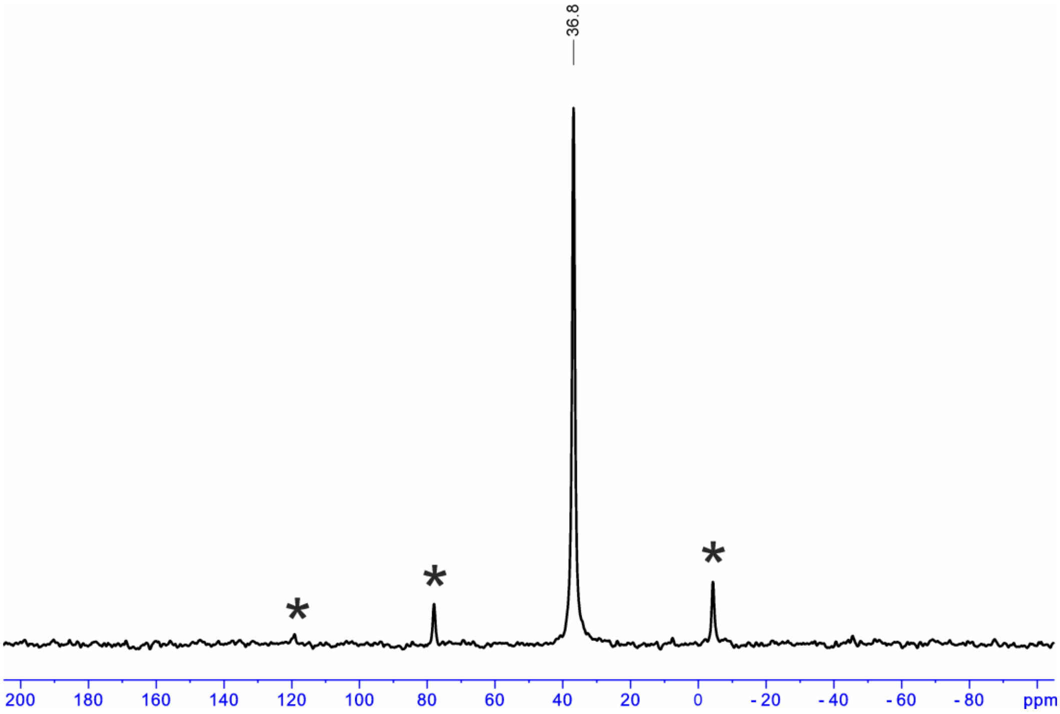

Fig. S48 ^{31}P CP-MAS NMR spectrum of **2b** (solid) recorded at spinning speed equal to 8kHz . Spinning sidebands were marked with asterisk.

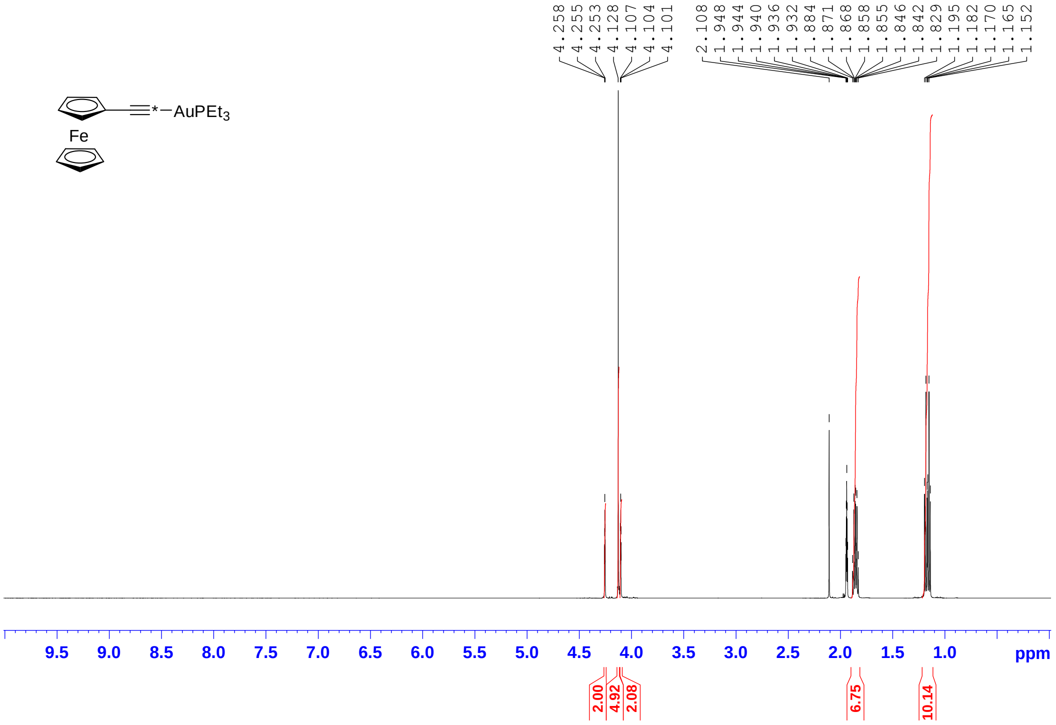

Fig. S49 ^{1}H NMR spectrum of ^{13}C-labeled **2b** (CD_3CN)

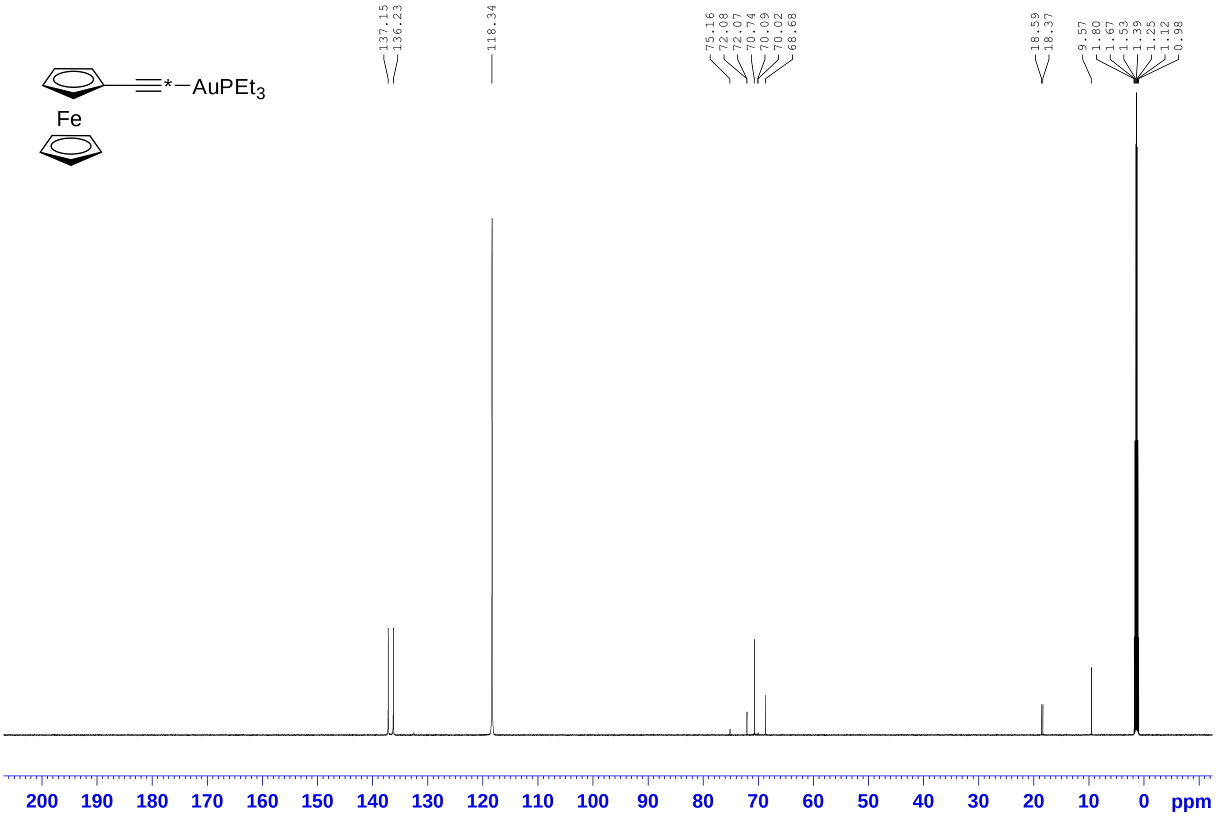

Fig. S50 ^{13}C{^{1}H} NMR spectrum of ^{13}C-labeled **2b** (CD_3CN)

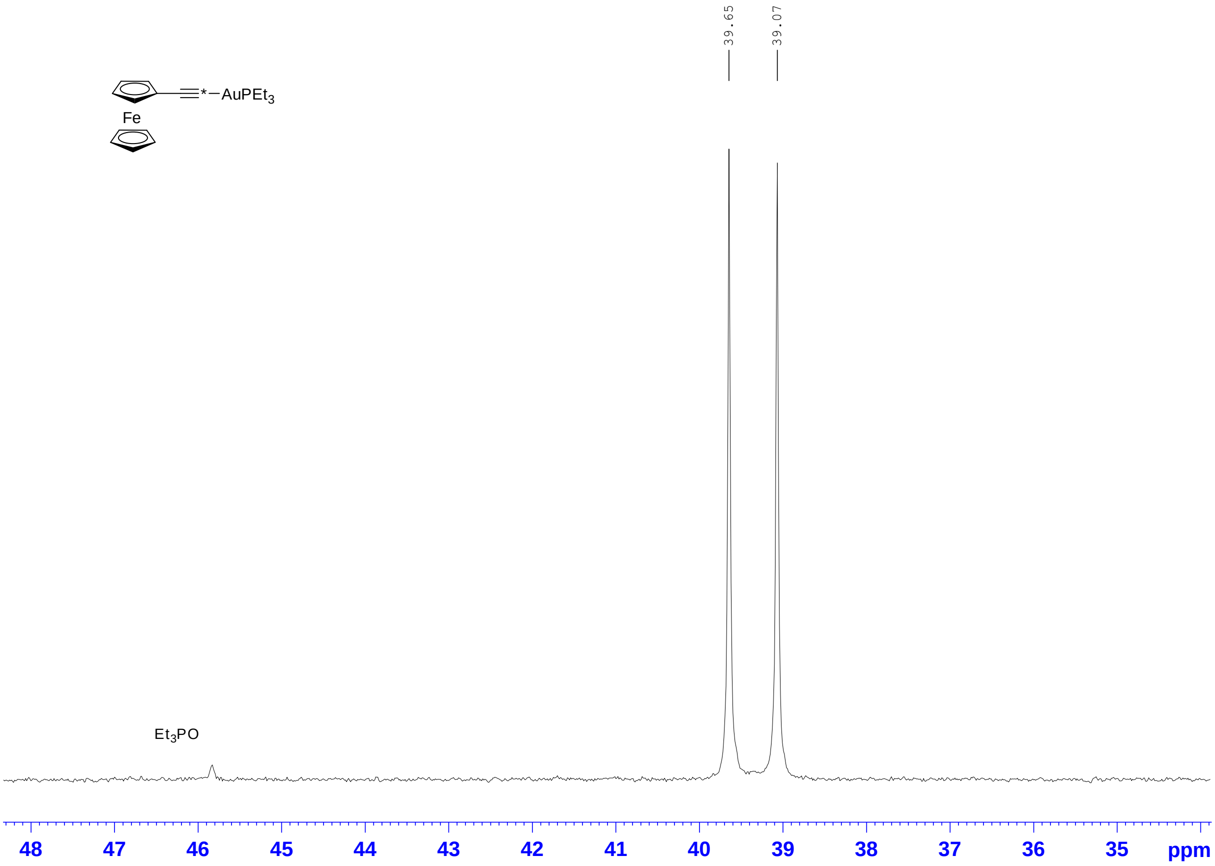

Fig. S51 $^{31}P\{^{1}H\}$ NMR spectrum of ^{13}C-labeled **2b** (CD_3CN)

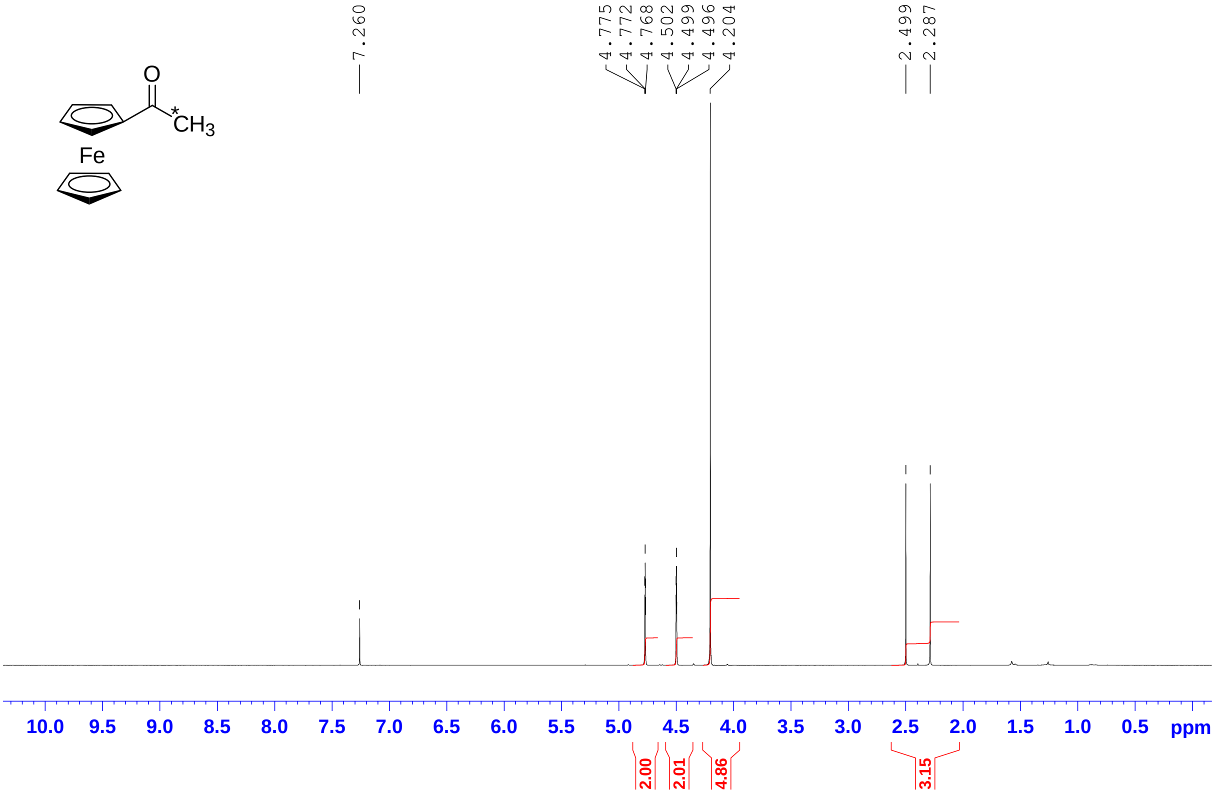

Fig. S52 ^{1}H NMR spectrum of **9** ($CDCl_3$)

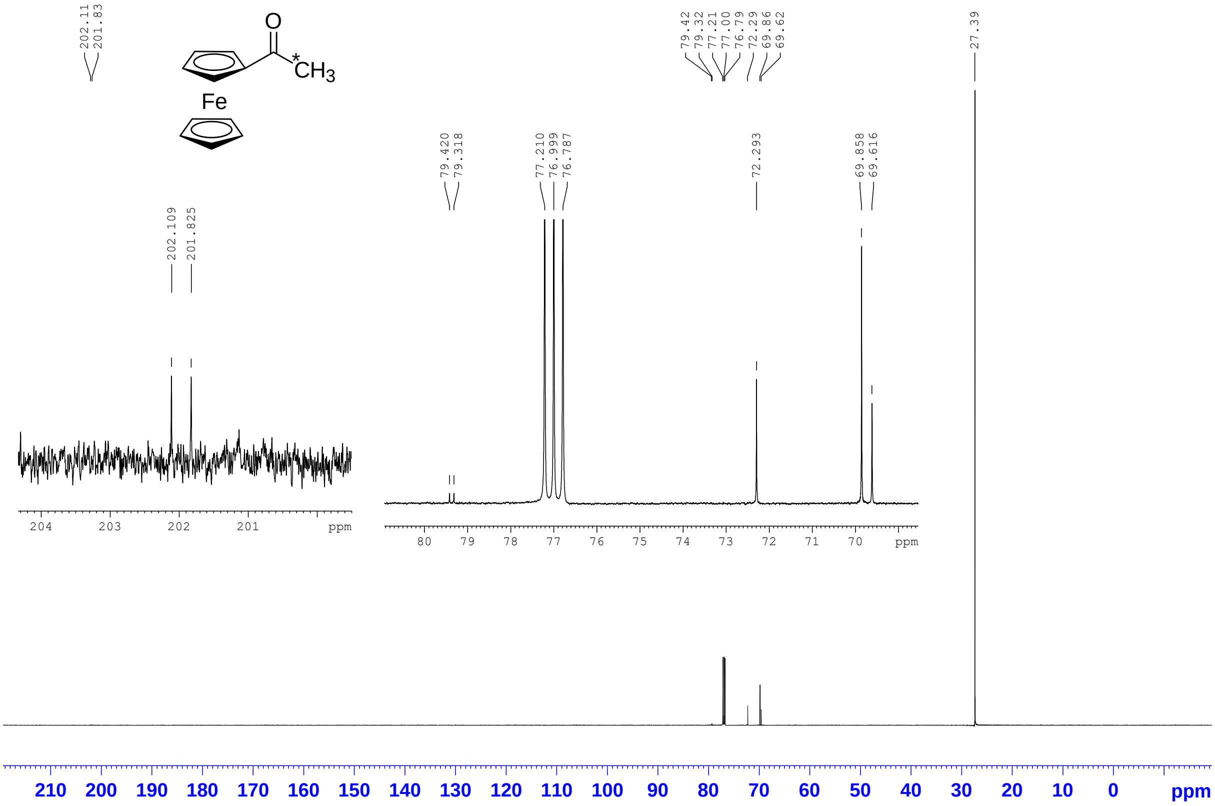

Fig. S53 $^{13}C\{^{1}H\}$ NMR spectrum of **9** ($CDCl_3$)

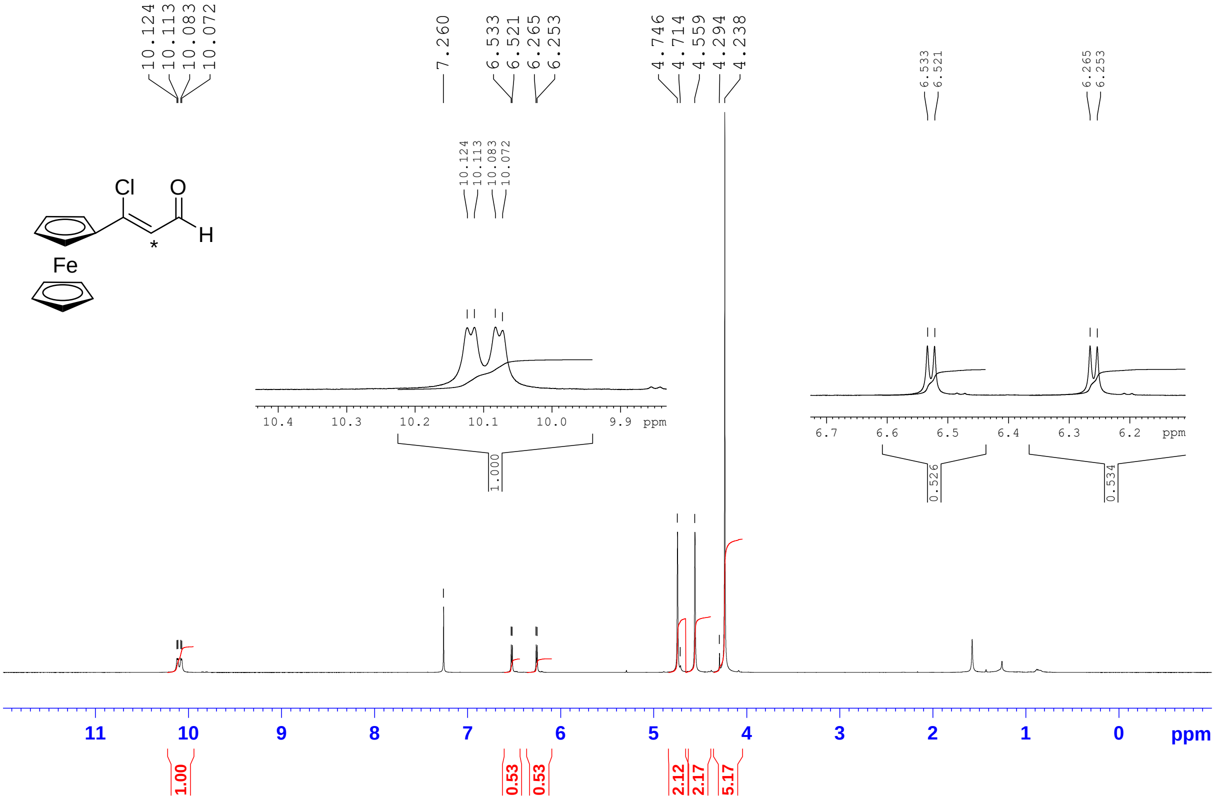

Fig. S54 ^{1}H NMR spectrum of **10** ($CDCl_3$)

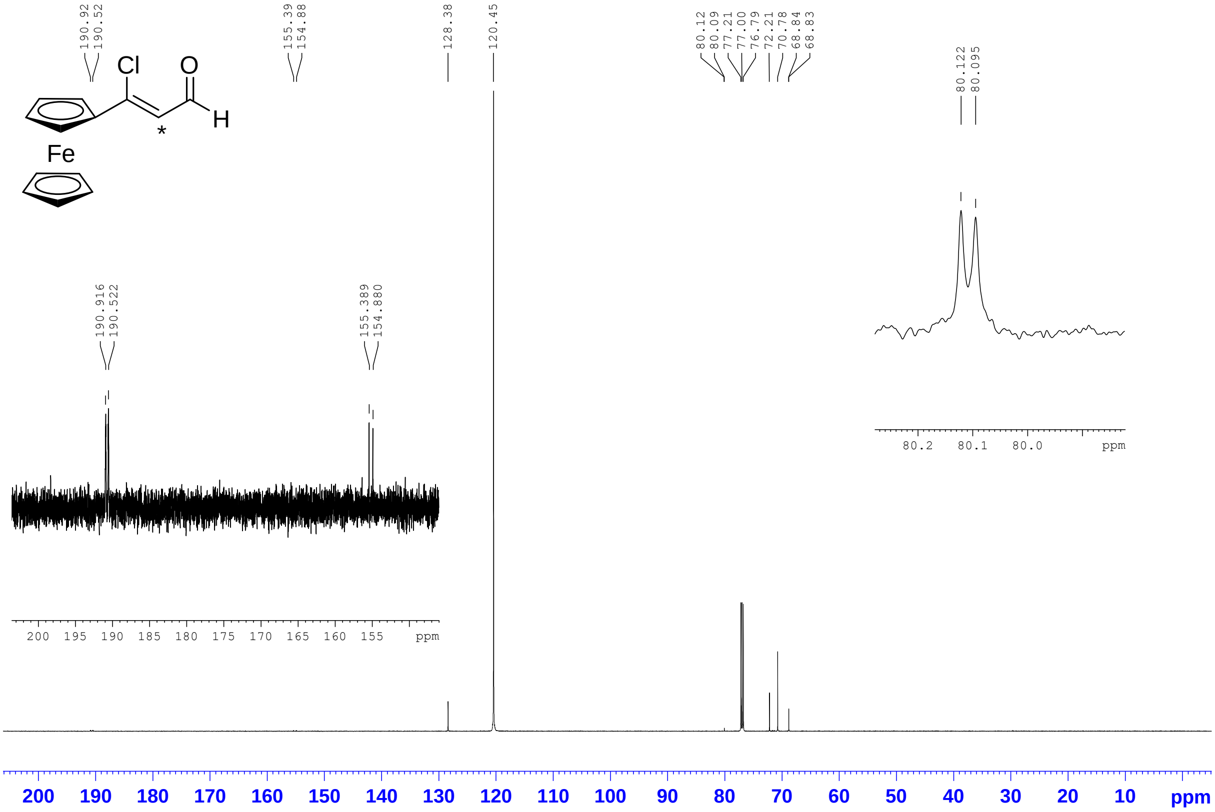

Fig. S55. $^{13}C\{^1H\}$ NMR spectra of **10** ($CDCl_3$)

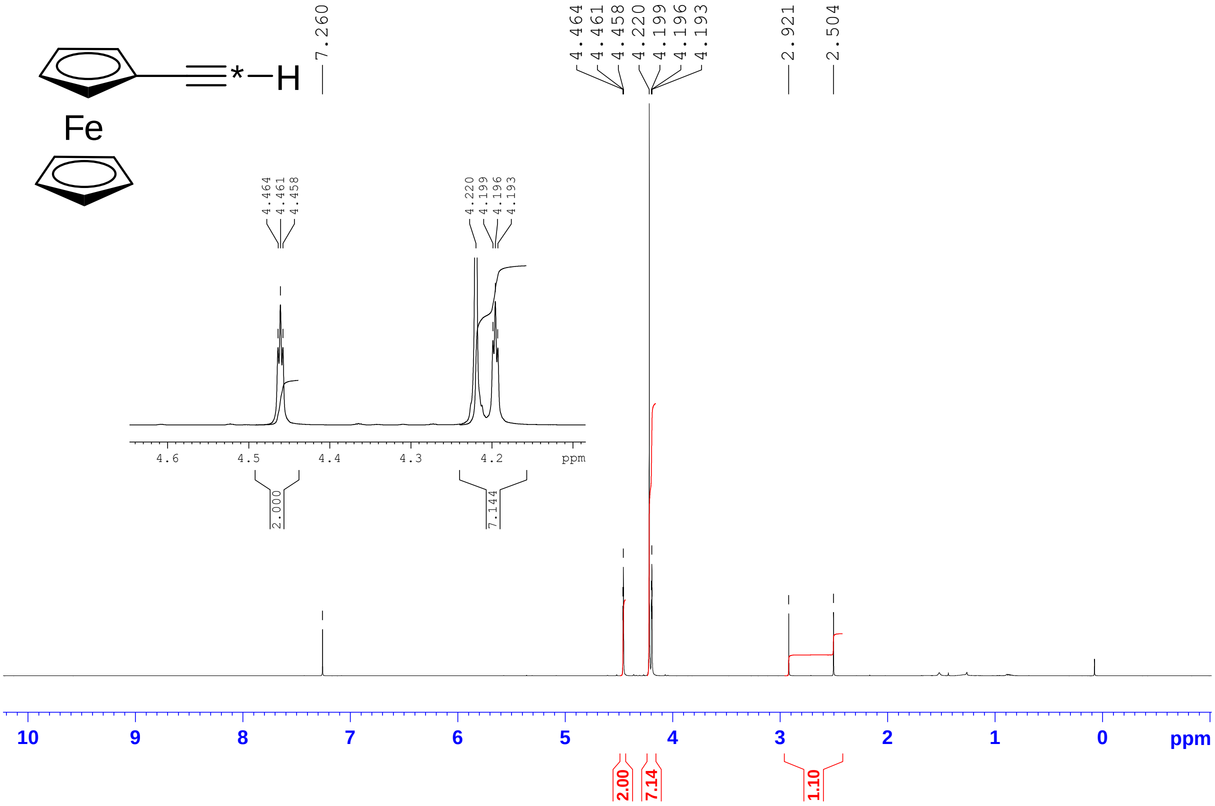

Fig. S56. ^1H NMR spectra of ^{13}C-labeled **4b** ($CDCl_3$)

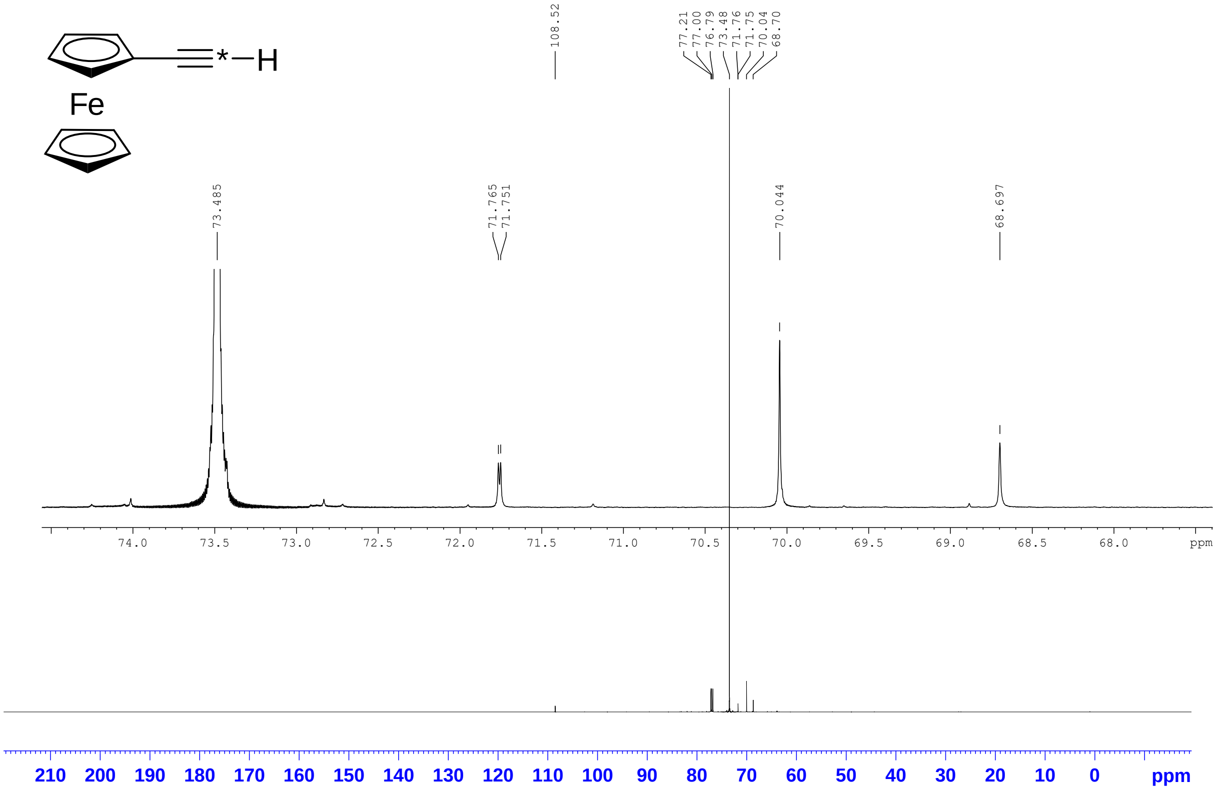

Fig. S57. $^{13}C\{^{1}H\}$ NMR spectra of ^{13}C-labeled **4b** ($CDCl_3$)

References

1. A. Lauber, B. Zelenay and J. Cvengros, *Chem. Commun.*, **2014**, 50, 1195-1197.
2. D. Plazuk and J. Zakrzewski, *J. Organomet. Chem.*, **2009**, 694, 1802-1806.
3. J. Polin and H. Schottenberger, *Organic syntheses*, **1996**, 73, 262-269.
4. APEX2 v2012.4-3 (Bruker AXS)
5. SAINT V8.18C (Bruker AXS Inc., **2011**)
6. SADABS-2008/1 (Bruker,2008)
7. CrysAlisPro 1.171.38.43d (Rigaku OD, **2015**)
8. Superflip (Palatinus & Chapuis, 2007;Palatinus & van der Lee, 2008; Palatinus et al., 2012)

9. G. Sheldrick, *Acta Cryst. A,* **2008**, 64, 112-122
10. O.V. Dolomanov, L.J. Bourhis, R.J. Gildea, J.A.K. Howard, H. Puschmann, *J. Appl. Cryst.*, **2009**, 42, 339-341
11. Farrugia, L. J. J. *Appl. Cryst*. **2012**, 45, 849
12. C. F. Macrae, P. R. Edgington, P. McCabe, E. Pidcock, G. P. Shields, R. Taylor, M. Towler and J. van de Streek, *J. Appl. Cryst*., **2006**, 39, 453-457
13. A. Hormann, C. Shaw III, D. Bennett and W. Reiff, I*norg. Chem.,* **1986**, 25, 3953-3957.
14. T. P. Seifert, A. C. Boukis, T. J. Feuerstein and P. W. Roesky, J. *Organomet. Chemis.,* **2017**, http://dx.doi.org/10.1016/ j.jorganchem.2017.09.023